

# Evolutionary Monte Carlo of QM properties in chemical space: Electrolyte design

Konstantin Karandashev,<sup>\*,†</sup> Jan Weinreich,<sup>†</sup> Stefan Heinen,<sup>‡</sup> Daniel Jose Arismendi Arrieta,<sup>¶</sup> Guido Falk von Rudorff,<sup>§,||</sup> Kersti Hermansson,<sup>¶</sup> and O. Anatole von Lilienfeld<sup>‡,⊥,#</sup>

<sup>†</sup>*University of Vienna, Faculty of Physics, Kolingasse 14-16, AT-1090 Wien, Austria*

<sup>‡</sup>*Vector Institute for Artificial Intelligence, Toronto, ON, M5S 1M1, Canada*

<sup>¶</sup>*Department of Chemistry-Ångström Laboratory, Uppsala University, Box 538, SE-75121 Uppsala, Sweden*

<sup>§</sup>*University Kassel, Department of Chemistry, Heinrich-Plett-Str.40, 34132 Kassel, Germany*

<sup>||</sup>*Center for Interdisciplinary Nanostructure Science and Technology (CINaT), Heinrich-Plett-Straße 40, 34132 Kassel*

<sup>⊥</sup>*Departments of Chemistry, Materials Science and Engineering, and Physics, University of Toronto, St. George Campus, Toronto, ON, Canada*

<sup>#</sup>*Machine Learning Group, Technische Universität Berlin and Institute for the Foundations of Learning and Data, 10587 Berlin, Germany*

E-mail: konstantin.karandashev@univie.ac.at

## Abstract

Optimizing a target function over the space of organic molecules is an important problem appearing in many fields of applied science, but also a very difficult one due to the vast number of possible molecular systems. We propose an Evolutionary Monte Carlo algorithm for solving such problems which is capable of straightforwardly tuning both exploration and exploitation characteristics of an optimization procedure while retaining favourable properties of genetic algorithms. The method, dubbed MOSAiCS (**M**etropolis **O**ptimization by **S**ampling **A**daptively in **C**hemical **S**pace), is tested on problems related to optimizing components of battery electrolytes, namely minimizing solvation energy in water or maximizing dipole moment while enforcing a lower bound on the HOMO-LUMO gap; optimization was done over sets of molecular graphs inspired by QM9 and Electrolyte Genome Project (EGP)

datasets. MOSAiCS reliably generated molecular candidates with good target quantity values, which were in most cases better than the ones found in QM9 or EGP. While the optimization results presented in this work sometimes required up to  $10^6$  QM calculations and were thus only feasible thanks to computationally efficient *ab initio* approximations of properties of interest, we discuss possible strategies for accelerating MOSAiCS using machine learning approaches.

## 1 Introduction

Increasing efficiency and longevity of energy storage systems is critical for improving economic sustainability of lowering greenhouse gas emissions.<sup>1</sup> One aspect of this problem is searching chemical compound space for organic molecules optimal for a target application, such as lithium battery electrolyte component<sup>2-6</sup> or

electroactive molecules for redox flow batteries.<sup>7,8</sup> In this work we focused on the former, more specifically on finding electrochemically stable organic molecules that are good solvents for alkali salts. While such searches can be aided with high-throughput screening,<sup>2-4</sup> there has been a surge of ways to go beyond by increasing efficiency of compound property evaluations, *e.g.* with machine learning<sup>9</sup> or quantum alchemy,<sup>10-12</sup> and by sampling chemical space more efficiently. In the context of optimizing small organic molecules, most methods of the latter category can be classified as those based on Markov decision processes,<sup>13-18</sup> recurrent neural networks,<sup>19,20</sup> genetic algorithms,<sup>21-26</sup> and variational autoencoders.<sup>27,28</sup>

While several variants of Markov chain Monte Carlo<sup>29</sup> sampling have also been applied to molecule optimization problems,<sup>30,31</sup> one intriguing variant, namely Evolutionary Monte Carlo,<sup>32-34</sup> has been overlooked so far. The approach combines two philosophies that have demonstrated reliable performance for a range of optimization problems: parallel tempering<sup>35-37</sup> and genetic algorithms.<sup>38-40</sup> As illustrated in Figure 1, Evolutionary Monte Carlo involves running several Markov chain Monte Carlo simulations that focus on *exploitation* (*i.e.* refining already known molecules via incremental changes) or *exploration* (*i.e.* finding promising regions of chemical space), which interact by swapping configurations analogously to parallel tempering or by creating "child configurations" similarly to genetic algorithms in a way that observes detailed balance condition.<sup>41</sup> As is the case for genetic algorithms, increasing the number of replicas yields more opportunities for creating "child configurations," thus accelerating exploration of chemical space. Unlike genetic algorithms though, Evolutionary Monte Carlo allows straightforward control of its exploration and exploitation aspects while guaranteeing to *eventually* find the global minimum due to the properties of Markov chain Monte Carlo. Evolutionary Monte Carlo can also potentially be combined with nested Monte Carlo techniques<sup>42-44</sup> to utilize multiple optimized quantity evaluation methods at once, *e.g.* when laboratory experiments are used

alongside theoretical and machine learning approaches,<sup>45-48</sup> an advantage particularly relevant for high-throughput automated laboratory workflows.<sup>48-51</sup>

With these reasons in mind, we implemented an Evolutionary Monte Carlo algorithm inspired by a family of genetic algorithms for optimization in the space of molecular graphs.<sup>21-24</sup> While some recently proposed methods for molecular optimization operate in string representations,<sup>18,19,25,52,53</sup> we performed all procedures directly on chemical graphs to facilitate ensuring validity of generated molecules and maintaining detailed balance, as well as provide a more direct connection between the molecules considered and graph-based representations that have proven efficient in machine learning applications.<sup>54,55</sup> Lastly, we implemented a simple Wang-Landau biasing potential<sup>56</sup> as a *curiosity reward*<sup>57</sup> increasing exploration aspect of the algorithm by "pushing" our Markov chain Monte Carlo simulations out of previously occupied graphs. The resulting method is named MOSAiCS (**M**etropolis **O**ptimization by **S**ampling **A**daptively in **C**hemical **S**pace). While we were mainly designing our approach with battery applications in mind, we think it should be useful for other molecular optimization problems, such as those arising in drug design.<sup>15,17,19,31,58-60</sup>

The rest of the paper is organized as follows. Section 2 presents the main ideas behind our approach in Subsecs. 2.1-2.3, following up with description of the optimization problem on which we test it in Subsec. 2.4 and details of our Monte Carlo simulations in Subsec. 2.5. Section 3 discusses our experimental results, Section 4 concludes the paper with a results summary and outline of possible strategies to improve our approach. Some technical details of our method’s implementation, experimental setup, and results were left for Supporting Information.

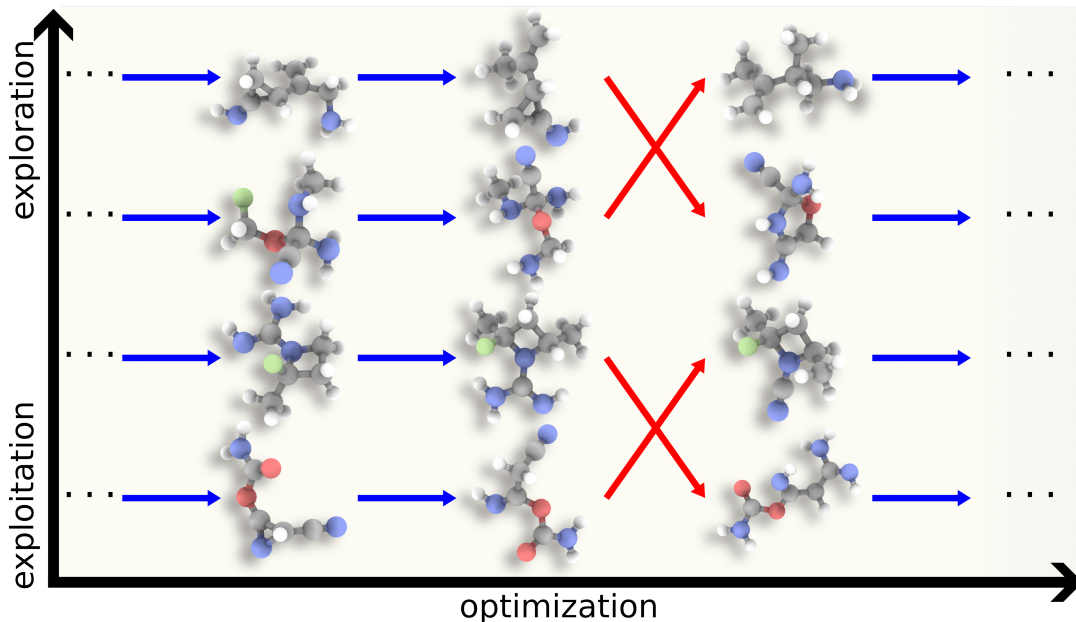


Figure 1: Scheme of an Evolutionary Monte Carlo workflow for molecular optimization that introduces several *replicas* with varying degree of focus on *exploitation* or *exploration* aspects of the calculation and evolves them by applying *elementary mutations* (blue) to single replicas and *crossover moves* (red) to pairs of replicas in a way satisfying detailed balance.

## 2 Theory

### 2.1 Chemical space definition

We aim to minimize a loss function  $F$  over a set of molecules, the latter represented by their *chemical graphs*. We define a chemical graph as an undirected graph whose *nodes* correspond to heavy atoms, along with, where present, hydrogen atoms covalently connected to them, and whose *edges* connect a pair of nodes if their heavy atoms share a covalent bond. For a chemical graph we also define a *resonance structure* as a set of *valences* of nodes’ heavy atoms and *orders of covalent bonds* connecting these heavy atoms, both quantities taking integer values. The sum of covalent bond orders connecting a heavy atom to other atoms equals its valence, with the orders of bonds between a heavy atom and a hydrogen atom counted as one. Valence numbers are chosen to be chemically reasonable (*e.g.* IV for C, II, or IV, or VI for S) and we require their sum to be the minimum needed to build a set of covalent bond orders. We also forbid a covalent bond order to be larger than three. The reasons for not including valences and bond orders in the definition of a chemi-

cal graph, but rather enumerating their possible values separately, are illustrated in Figure 2 demonstrating examples of molecules for which several resonance structures differing in bond orders or bond orders and heavy atom valences can be defined. We emphasize that while this definition of bond orders and valences is loosely based on valence structure theory, it was designed not to reflect actual electronic structure of a molecule, but to allow convenient definitions of changes of chemical graphs that are illustrated in Figures 3 and 4, as will be discussed in detail in Subsec. 2.3.

Our definition of chemical graph *a priori* prevents us from differentiating between conformers or stereoisomers and we will assume our optimization problem to be unaffected by this, *e.g.* if for a given chemical graph we are interested only in the most stable stereoisomer and we optimize a Boltzmann average. We also did not implement support for molecules where valid Lewis structures can only be generated by assigning charges to atoms, *e.g.* compounds with nitro groups, hence they were ignored during all calculations done in this work.

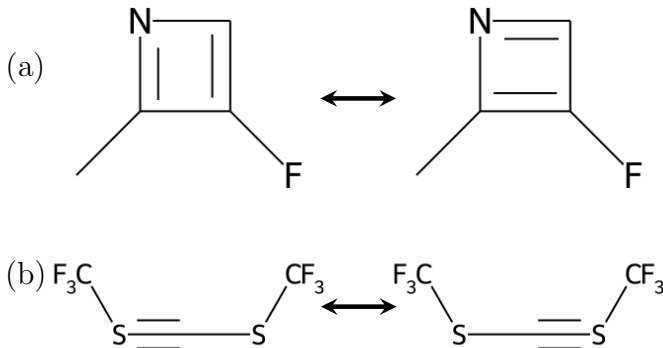


Figure 2: Examples of molecules that can be written in terms of several resonance structures that differ in (a) covalent bond orders and (b) both covalent bond orders and heavy atom valences.

## 2.2 Monte Carlo sampling

We perform optimization by running a Markov chain Monte Carlo simulation (referred to as just “simulation” from now on) of unnormalized probability density similar to the one used for parallel tempering

$$P(\mathbf{X}) = \exp \left\{ - \sum_{i=1}^{N_{\text{opt}}} C^{\infty} [F(X^{(i)})] - \sum_{i=N_{\text{opt}}+1}^{N_{\text{repl}}} \beta^{(i)} [F(X^{(i)}) + V_{\text{bias}}^{(i)}(X^{(i)})] \right\}, \quad (1)$$

where  $\mathbf{X}$  is a set of  $N_{\text{repl}}$  chemical graphs (also referred to as *replicas*)  $X^{(i)}$  ( $i = 1, \dots, N_{\text{repl}}$ ),  $\beta^{(i)}$  ( $i = N_{\text{opt}} + 1, \dots, N_{\text{repl}}$ ) are temperature parameters,  $V_{\text{bias}}$  is biasing potential,  $C^{\infty}$  is the “infinitely convex function” defined to be such that for arbitrary sets of numbers  $x^{(j)}$  and  $y^{(j)}$  ( $j = 1, \dots, N_{\text{opt}}$ )

$$\min_{j=1, \dots, N_{\text{opt}}} x^{(j)} - \min_{j=1, \dots, N_{\text{opt}}} y^{(j)} < 0 \Leftrightarrow \sum_{j=1}^{N_{\text{opt}}} [C^{\infty}(x^{(j)}) - C^{\infty}(y^{(j)})] \rightarrow +\infty, \quad (2)$$

and  $N_{\text{opt}}$  is the number of replicas that, as will become clear later, effectively undergo greedy stochastic minimization and are referred to as

*greedy replicas*, with the other replicas, referred to as *exploration replicas*, providing a less restricted exploration of chemical space and preventing greedy replicas from getting stuck in a local minimum of  $F$ . The history-dependent biasing potential  $V_{\text{bias}}^{(i)}$  is defined as<sup>56</sup>

$$V_{\text{bias}}^{(i)}(X) = \frac{\alpha_b}{\beta^{(i)}} \sum_{j=N_{\text{opt}}+1}^{N_{\text{repl}}} \rho^{(j)}(X), \quad (3)$$

where  $\rho^{(j)}(X)$  is the number of times  $X$  has been visited during the simulation by replica with index  $j$  (details on how it was evaluated are left for Subsec. 2.5),  $\alpha_b$  is the user-defined bias proportionality coefficient. Setting a non-zero  $\alpha_b$  makes sampling  $\mathbf{X}$  non-Markovian; as a result our certainty that in this regime a global minimum of  $F$  w.r.t.  $X$  is eventually found is based not on properties of Markov chain Monte Carlo, but on heuristic expectation that the biasing potential would make probability distribution of each exploration replica approach uniformity, leading to at least one replica coming across the global minimum over a finite number of simulation steps.

## 2.3 Monte Carlo moves

A simulation consists of taking a sequence of *moves* in a way outlined in Algorithm 1. If the current set of replicas is in configuration  $\mathbf{X}_1$ , a move involves randomly generating parameters  $\mathbf{w}$  of a change and deciding to replace  $\mathbf{X}_1$  with the change’s outcome (or *trial configuration*)  $\mathbf{X}_2$  with an acceptance probability similar to the standard Metropolis-Hastings expression<sup>41</sup>

$$P_{\text{acc}}(\mathbf{X}_1, \mathbf{w}, \mathbf{X}_2) = \min \left[ 1, \frac{P_{\text{prop}}(\mathbf{X}_1, \mathbf{w}) P(\mathbf{X}_2)}{P_{\text{prop}}(\mathbf{X}_2, \mathbf{w}^{-1}) P(\mathbf{X}_1)} \right], \quad (4)$$

where  $P_{\text{prop}}(\mathbf{X}_1, \mathbf{w})$  is the probability that  $\mathbf{w}$  is proposed given that  $\mathbf{X}_1$  is the initial configuration and  $\mathbf{w}^{-1}$  are parameters of a random change yielding  $\mathbf{X}_1$  when applied to  $\mathbf{X}_2$  and corresponding to a unique  $\mathbf{w}$ . The latter property

ensures that detailed balance still holds in situations when several  $\mathbf{w}$  yield the same trial configuration  $\mathbf{X}_2$ . Trial configurations decreasing the minimal value of  $F$  among greedy replicas compared to initial configurations is accepted automatically due to our definition of  $C^\infty$  (2).

---

**Algorithm 1** Sampling  $P(\mathbf{X})$  (1).

---

**Require:** Initial configuration:  $\mathbf{X}_1$ ;  
**loop**  
 Randomly choose change parameters  $\mathbf{w}$ ;  
 Use  $\mathbf{w}$  on  $\mathbf{X}_1$  to generate  $\mathbf{X}_2$ ;  
 Randomly sample  $r$  from uniform distribution in  $[0, 1]$ ;  
 $r_{\text{acc.}} \leftarrow P_{\text{acc.}}(\mathbf{X}_1, \mathbf{w}, \mathbf{X}_2)$  (see Eq. (4));  
**if**  $r < r_{\text{acc.}}$  **then**  
 $\mathbf{X}_1 \leftarrow \mathbf{X}_2$ ;  
**end if**  
**end loop**

---

We use three types of moves to propose the trial configurations  $\mathbf{X}_2$ ; we will only discuss the general idea behind them here with implementation details left for Supporting Information. The first type, referred to as *elementary moves*, applies an *elementary mutation* outlined in Figure 3 to a single replica; such moves correspond to incremental exploration of chemical space. To accelerate greedy optimization of molecules, we additionally introduced the “no reconsiderations condition”: if change parameters  $\mathbf{w}$  corresponding to an elementary move have been rejected for a greedy replica they are not considered again. The second type of moves is *tempering swap* moves that are analogous to the swap moves in conventional parallel tempering techniques and involve randomly choosing replicas with indices  $i$  and  $j$  in such a way that at least one of them is an exploration replica, considering a swap of the corresponding chemical graphs, and accepting it with acceptance probability (4). These moves allow greedy replicas stuck in a local minimum of  $F$  to get to chemical graphs with lower values of  $F$  if the latter are discovered by an exploration replica.

The third type of moves are *crossover moves* inspired by the procedure developed in Ref. 21, which are introduced to allow drastic changes of chemical graphs occupied by replicas. The

general idea is illustrated in Figure 4: a pair of nodes is randomly chosen in two chemical graphs and the neighborhoods of these two nodes are exchanged to create two new chemical graphs. Thus defined crossover moves are more restrictive than the ones of Ref. 21 as they do not allow exchanging fragments of arbitrary shape and connectivity. These restrictions, however, make it straightforward to ensure that the resulting chemical graphs satisfy constraints on the number of nodes, are connected, and correspond to a change for which the  $P_{\text{prop}}(\mathbf{X}_1, \mathbf{w})/P_{\text{prop}}(\mathbf{X}_2, \mathbf{w}^{-1})$  ratio in  $P_{\text{acc}}$  (4) can be easily calculated.

Setting  $F$  to be infinitely large for chemical graphs violating certain user-defined constraints is a general way to enforce the latter on the optimization result. However, it is in general preferable to maintain a given constraint as early as during the proposition of trial configuration  $\mathbf{X}_2$  to increase average acceptance probability and the resulting speed of chemical space exploration. We implemented the corresponding algorithms for maintaining constraints on the number of heavy atoms in a molecule and the kinds of atoms that can share a covalent bond since they are simple to maintain, yet quite important for our applications. Lastly, the question of the moves’ sufficiency to access the chemical space and sets of molecules considered in Section 3 in their entirety is discussed in Supporting Information.

## 2.4 Minimization problems

A good battery electrolyte is a good solvent for lithium salts and is electrochemically stable. We approximated the former property with polarity; maximizing a molecule’s polarity was in turn approximated by either maximizing the dipole moment  $D$  or minimizing the free energy of solvation in water  $\Delta G_{\text{solv}}$ . We approximated the electrochemical stability requirement with a lower bound on the HOMO-LUMO  $\Delta\epsilon$ , with which we approximated the width of the compound’s electrochemical stability window.<sup>2</sup> While the latter relation is not actually practical for battery design,<sup>61</sup> we still opted for a  $\Delta\epsilon$ -based electrochemical stability criterion to

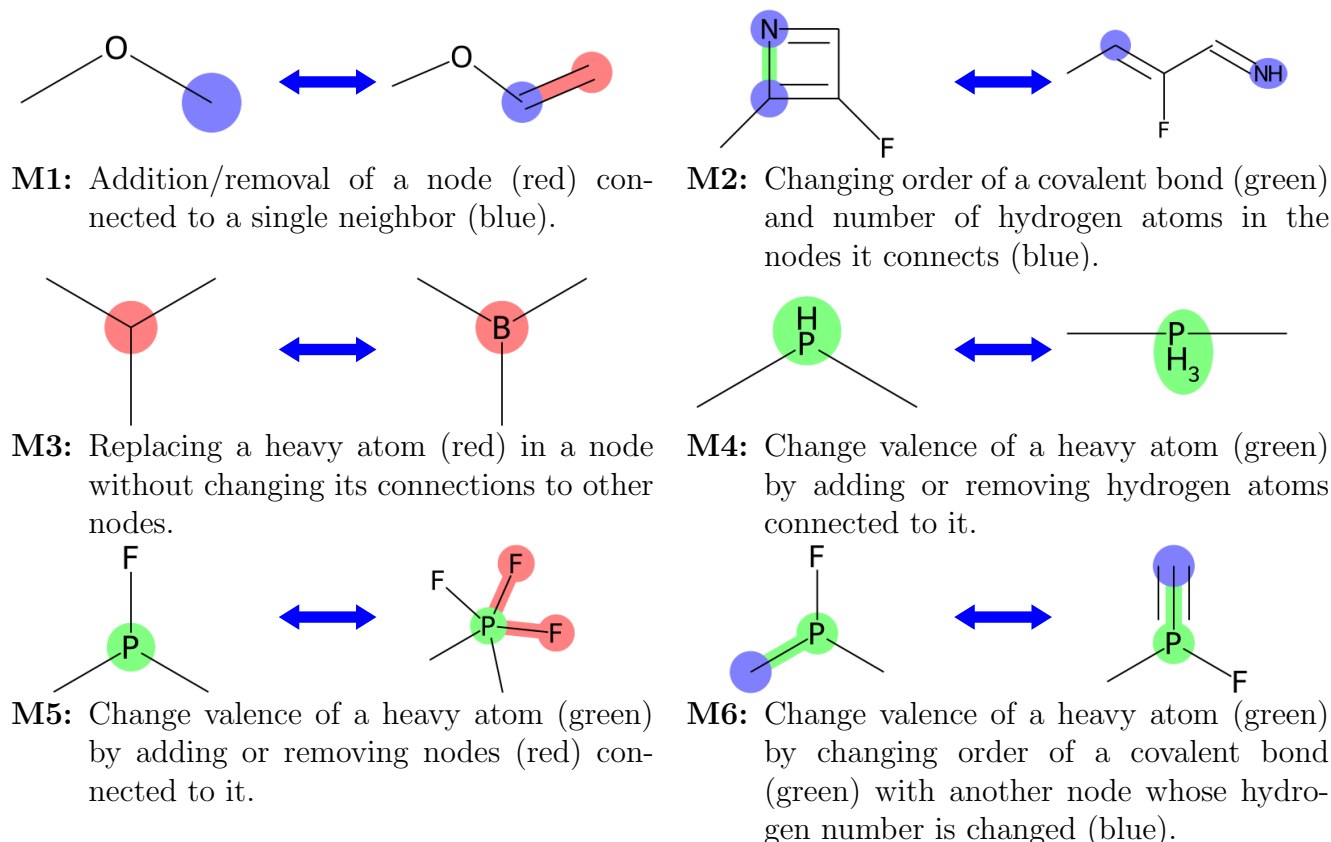


Figure 3: Definitions and examples of elementary mutations. A node is colored green if its heavy atom changes valence, otherwise it is colored red if it is destroyed or created, or colored blue if it changes the number of hydrogen atoms connected to the heavy atom. A bond is colored red if it is destroyed or created or green if it, in general, only changes bond order, though the latter may involve changing the order to and from 0. The valences in M5 and M6 always change to adjacent values (*e.g.* for S valence can change from II to IV, but not from II to VI); nodes created and destroyed in M1, M3, and M5 contain heavy atoms in their smallest valence state (*e.g.* valence II for S).

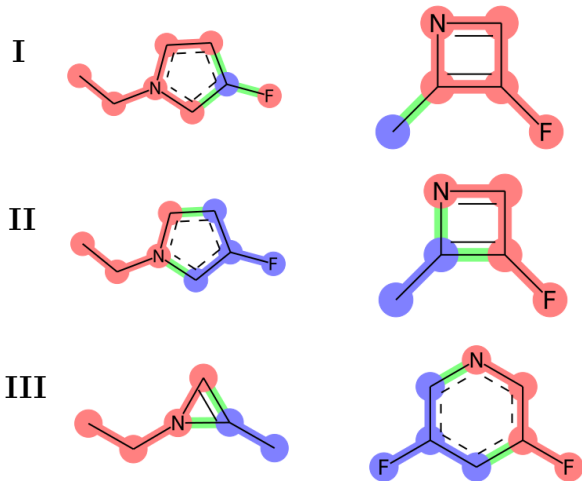


Figure 4: An example of a crossover move. I - selection of two “blue” nodes in two molecules; II - selecting the “blue” neighborhoods of the two blue nodes, coloring the rest “red,” with the bonds connecting blue and red fragments colored “green”; III - exchanging the blue fragments between molecules and reconnecting them with red fragments by exchanging connected nodes between pairs of green bonds.

connect our work with other compound optimization problems where  $\Delta\epsilon$  can be used.<sup>62,63</sup> For both  $D$  and  $\Delta G_{\text{solv}}$  optimization we constrained the molecules’  $\Delta\epsilon$  to be larger than either benzene (*strong  $\Delta\epsilon$  constraint*) or octa-1,3,5,7-tetraene (*weak  $\Delta\epsilon$  constraint*), resulting in four minimization problems of differing difficulty. While in this work we focused on testing performance of MOSAiCS against these single objective optimization problems, our approach can also be used to optimize several properties at once via a suitable multiobjective loss function.<sup>64</sup>

We aimed to estimate  $\Delta G_{\text{solv}}$ ,  $D$ , and  $\Delta\epsilon$  as computationally cheaply as possible while being qualitatively correct over a wide range of chemical compounds; the resulting protocol is explained in detail in Supporting Information. Here we just mention that for a given chemical graph we used the MMFF94 forcefield<sup>65</sup> to generate molecular conformers, for which we performed GFN2-xTB<sup>66</sup> calculations with analytical linearized Poisson-Boltzmann model<sup>67</sup> simulating presence of water. The root mean square error (RMSE) that is presented for cal-

culated quantities corresponds to statistical error from randomness of conformer generation. We used two sets of parameters for our protocol: “converged” that produced reasonable RMSEs for a wide variety of compounds, but was relatively computationally expensive, and “cheap” that was used during our simulations. From now on,  $\Delta G_{\text{solv}}$ ,  $D$ , and  $\Delta\epsilon$  will denote estimates of these quantities obtained with the “converged” protocol, while estimates obtained with the “cheap” protocol will be marked with addition of “cheap” superscript.

Each of the four minimization problems was solved in two sets of molecules based on QM9<sup>68</sup> and the Electrolyte Genome Project<sup>5</sup> (EGP) datasets. The QM9 dataset consists of 134k molecules containing up to 9 heavy atoms (C, O, N, and F). We defined the “QM9\*” set to consist of molecules (not necessarily in QM9) that also contain up to 9 heavy atoms of the same elements as QM9, but are additionally constrained by not allowing bonds between N, O, and F atoms, as well as O-H and H-F bonds, since these covalent bonds are typically associated with increased chemical reactivity. The EGP dataset was generated with the Materials Project<sup>69</sup> workflows in an effort to facilitate discovery of novel battery electrolyte molecules; the version currently hosted on the Materials Project website contains 24.5k species in total; neutral species for which MMFF94 coordinates could be generated included 19.7k individual chemical graphs containing up to 92 heavy atoms. These characteristics of the EGP dataset were the basis for defining the “EGP\*” set, whose molecules (not necessarily in EGP) contain up to 15 heavy atoms (B, C, N, O, F, Si, P, S, Cl, and Br, which are elements present in organic molecules of EGP) and, for the sake of chemical stability, do not contain covalent bonds between N, O, F, Cl, and Br, between H and B, O, F, Si, P, S, Cl, or Br, as well as S-S and P-P bonds.

We chose 15 as the maximum number of heavy atoms allowed in EGP\* molecules because this size restriction is obeyed by 87.0% and 97.0% of EGP’s chemical graphs satisfying weak and strong  $\Delta\epsilon$  constraints. When choosing which elements can not share a covalent

bond in QM9\* and EGP\* molecules we mainly aimed for excluding weak bonds, although we also forbade some relatively strong bonds whose presence can signify molecular reactivity. Since we only consider molecules whose valid Lewis structures can be generated without assigning charges to atoms, H-F and double O-O bonds can only be encountered in hydrogen fluoride and oxygen, which we excluded from consideration due to their corrosive properties. Creating N-N bonds inside an organic compound risks making it prone to releasing nitrogen on excitation, adding functional groups containing double N-O bonds to a molecule risks making the latter prone to self-oxidation, and hydroxyl groups engage relatively easily in reactions involving oxidation or nucleophilic attacks.<sup>70</sup> We note that in practice, managing this kind of reactive behavior would require additional use of more sophisticated compound stability measures.

While both QM9\* and EGP\* are well defined and finite sets of chemical graphs, their huge size makes evaluating any of their properties exactly, *i.e.* through exact enumeration of all their chemical graphs, unfeasible. However, we do summarize properties of intersections of QM9\* and QM9, as well as EGP\* and EGP, in Supporting Information.

## 2.5 Simulation details

During a simulation we used  $\Delta\epsilon^{\text{cheap}}$  to estimate whether a molecule satisfies the constraint on  $\Delta\epsilon$ ; dimensionless loss functions corresponding to  $D$  and  $\Delta G_{\text{solv}}$  were defined as

$$F_{\text{solv.}}(X) = \frac{\Delta G_{\text{solv}}^{\text{cheap}}(X)}{\text{STD}_{\text{dataset}}(\Delta G_{\text{solv}})}, \quad (5)$$

$$F_{\text{dipole}}(X) = -\frac{D^{\text{cheap}}(X)}{\text{STD}_{\text{dataset}}(D)}, \quad (6)$$

where  $\text{STD}_{\text{dataset}}$  refers to standard deviation of a quantity over molecules at the intersection of chemical graph set of interest and the reference dataset (QM9 for QM9\* and EGP for EGP\*) which satisfy the  $\Delta\epsilon$  constraint of interest. We chose 1000 "pre-final" molecules exhibiting the smallest value of loss function out

of the molecules visited during the simulation and evaluated converged estimates of the quantities of interest for them; the molecule with the best  $D$  or  $\Delta G_{\text{solv}}$  value among pre-final molecules satisfying the  $\Delta\epsilon$  constraint is the one considered the *candidate* molecule proposed by the simulation.

We used  $N_{\text{repl}} = 36$  with  $N_{\text{opt}} = 4$  (cf. definitions in Subsection 2.2); virtual temperature parameters  $\beta^{(i)}$  appearing in  $P$  (1) were defined in such a way that the smallest and largest  $\beta^{(i)}$  were 1 and 8, and the other  $\beta^{(i)}$  formed a geometric progression between the two extrema values, the latter being a simple recipe taken from applications of parallel tempering to configuration space sampling.<sup>71,72</sup> A simulation consisted of 50000 "global" steps, out of which 60% were "simple" steps applying an elementary move to each replica, 20% were "tempering" steps making tempering swap moves on 128 randomly chosen pairs of replicas, and another 20% were "crossover" steps making crossover moves on 32 randomly chosen pairs of replicas.  $\rho^{(j)}(X)$  appearing in  $V_{\text{bias}}^{(i)}$  (3) was counted as the number of times replica  $j$  was found in  $X$  after a global step had been completed. For elementary moves we additionally set that: the nodes added or removed during M1 mutation could be connected to the molecule with bonds of order from 1 to 3; bonds changed with M2 and M6 mutations could have their order increased or decreased by 1 and 2 respectively; nodes added or removed with M5 mutation could be connected to the molecule with bonds of order 1 or 2.

We set  $\alpha_b$  to 0.0, 0.2, or 0.4; for each of the resulting 12 combinations of  $\alpha_b$  and optimization problem we ran 8 simulations with different random number generator seeds. For all simulations all replicas initially occupied the chemical graph of methane. While it would be natural to assign each replica a randomly chosen molecule from the intersection of QM9 and QM9\* or EGP and EGP\*, we went with the intentional handicap of using methane as the starting molecule to demonstrate that MO-SAiCS is capable of constructing all the candidate molecules presented in this Section from scratch. The effect of choice of initial condi-



tions on the final result is briefly addressed in Supporting Information.

### 3 Results and discussion

In this Section we describe the main results of our numerical experiments. The more technical aspects, such as full information on generated candidates and influence of biasing potential on search efficiency, are left for Supporting Information.

While we ran in total 96 simulations in QM9\*, or 24 simulations with different random generator seed and  $\alpha_b$  values for each optimization problem, they agreed remarkably often on candidates proposed, only yielding 10 candidates in total. Table 1 summarizes the best and worst values of optimized quantities of candidates proposed by MOSAiCS along with the corresponding relative improvement, which we define as absolute difference between a candidate’s optimized quantity value and the corresponding value for the best molecule for the optimization problem taken from the reference dataset (cf. Table S2 in Supporting Information), divided by the corresponding  $\text{STD}_{\text{dataset}}$ . For optimization of  $\Delta G_{\text{solv}}$  with weak  $\Delta\epsilon$  constraint all trajectories proposed the minimum of  $\Delta G_{\text{solv}}$  already present in QM9, while for all other optimization problems all trajectories proposed candidates that improved significantly on molecules in QM9. Best candidates proposed for a given optimization problem are shown in Figure 5; note that to facilitate discussion of candidates’ properties in Supporting Information, each candidate is referred by a capital  $C$  with a unique index subscript and a superscript denoting the reference dataset. We see how MOSAiCS successfully constructed complex conjugated bond structures facilitating charge transfer which, in turn, led to smaller, *i.e.* more negative,  $\Delta G_{\text{solv}}$  or larger  $D$ . Figure 6 displays optimization progress with number of global Monte Carlo steps for different  $\alpha_b$  values for minimizing  $\Delta G_{\text{solv}}$  with weak  $\Delta\epsilon$  constraint. We observe convergence of the optimized property with a rate not significantly affected by changing  $\alpha_b$ ; the same is true with

varying degree for other optimization problems as discussed in Supporting Information. To visualize how simulations explored chemical space for different optimization problems and values of  $\alpha_b$ , for each such combination we took a simulation that had produced the best candidate and plotted the density of molecules it encountered with respect to the optimized quantity and  $\Delta\epsilon$ . Figure 7 presents such plots for minimizing  $\Delta G_{\text{solv}}$  with weak  $\Delta\epsilon$  constraint, with plots for other optimization problems presented and discussed in Supporting Information. We see that increasing  $\alpha_b$  tended to increase diversity of molecules encountered during the simulations, but this was mainly done by considering more molecules in regions of chemical space with larger values of  $\Delta G_{\text{solv}}$ .

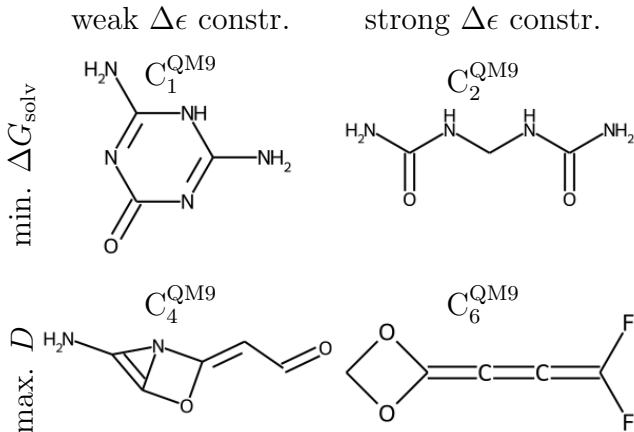


Figure 5: QM9\* candidates that exhibited smallest free energy of solvation  $\Delta G_{\text{solv}}$  or largest dipole  $D$  under weak or strong constraint on the HOMO-LUMO gap  $\Delta\epsilon$ . See Supporting Information for more information about them.

Optimization in EGP\* was harder than in QM9\* due to larger size of the former set of molecules, resulting in our protocol generating underconverged simulations that rarely agreed on candidates, producing 83 candidates in total. However, as summarized in Table 2, we still observed significant improvement of optimized quantities compared to EGP, though the improvements’ impressive magnitudes are largely due to EGP containing a much less representative portion of EGP\* compared to the case

Table 1: Best and worst QM9\* candidates proposed during minimization of free energy of solvation  $\Delta G_{\text{solv}}$  or maximization of dipole  $D$  with weak or strong constraint on the HOMO-LUMO gap  $\Delta\epsilon$ , along with their optimized quantity values and the relative improvement compared to QM9 dataset as defined in Sec. 3.  $\Delta G_{\text{solv}}$  and  $D$  values are in kJ/mol and debye. The full list of candidate molecules can be found in Supporting Information.

optimized quantity	$\Delta\epsilon$ constraint	optimized quantity value		relative improvement	
		best	worst	best	worst
$\Delta G_{\text{solv}}$	weak	$-94.79 \pm 0.06$	-	$0.004 \pm 0.009$	-
	strong	$-68.19 \pm 0.60$	$-67.27 \pm 0.00$	$1.665 \pm 0.099$	$1.537 \pm 0.052$
$D$	weak	$15.73 \pm 0.10$	$15.23 \pm 0.00$	$1.287 \pm 0.052$	$1.013 \pm 0.000$
	strong	$11.14 \pm 0.00$	$10.00 \pm 0.00$	$1.924 \pm 0.030$	$1.087 \pm 0.030$

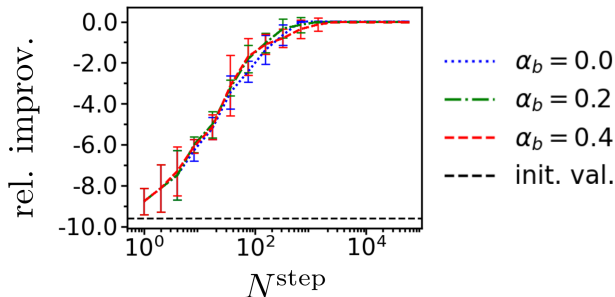


Figure 6: Relative improvement (as defined in Subsec. 3 and estimated from  $\Delta G_{\text{solv}}^{\text{cheap}}$ ) observed at  $N^{\text{step}}$  global Monte Carlo steps for QM9\* simulations optimizing  $\Delta G_{\text{solv}}$  with weak  $\Delta\epsilon$  constraint. For each bias proportionality coefficient  $\alpha_b$  we plot the mean over different random generator seeds, the error bars corresponding to standard deviation. "init. val." is the relative improvement of the simulations' starting molecule, *i.e.* methane.

of QM9 and QM9\*. Best EGP\* candidates for each optimization problem are presented in Figure 8; unlike QM9\* candidates, no chemical intuition is seen in how they were constructed beyond adding as many polar covalent bonds as possible, which may be due to underconvergence of our EGP\* simulations. The underconvergence can also be observed on our optimization progress plots, the plot for minimizing  $\Delta G_{\text{solv}}$  with weak  $\Delta\epsilon$  constraint presented in Figure 9 and the rest found in Supporting Information. Figure 9 also demonstrates how adding  $\alpha_b$  can accelerate optimization as a function of global Monte Carlo steps, though we need to note that simulations with larger  $\alpha_b$  on average process more chemical graphs per global Monte Carlo steps as discussed in Supporting Information. Densities of molecules encountered during simulations minimizing  $\Delta G_{\text{solv}}$  with weak  $\Delta\epsilon$  constraint that produced the best candidates are presented in Figure 10; unlike the case of QM9\*, increasing  $\alpha_b$  helped simulations explore parts of chemical space with smaller values of  $\Delta G_{\text{solv}}$ . Analogous plots for other optimization problems in EGP\* are presented in Supporting Information.

## 4 Conclusions and outlook

We have proposed an effective algorithm for optimization in chemical space, dubbed MO-SAiCS, and successfully applied it to several test optimization problems connected to lithium battery electrolyte design. In the cur-

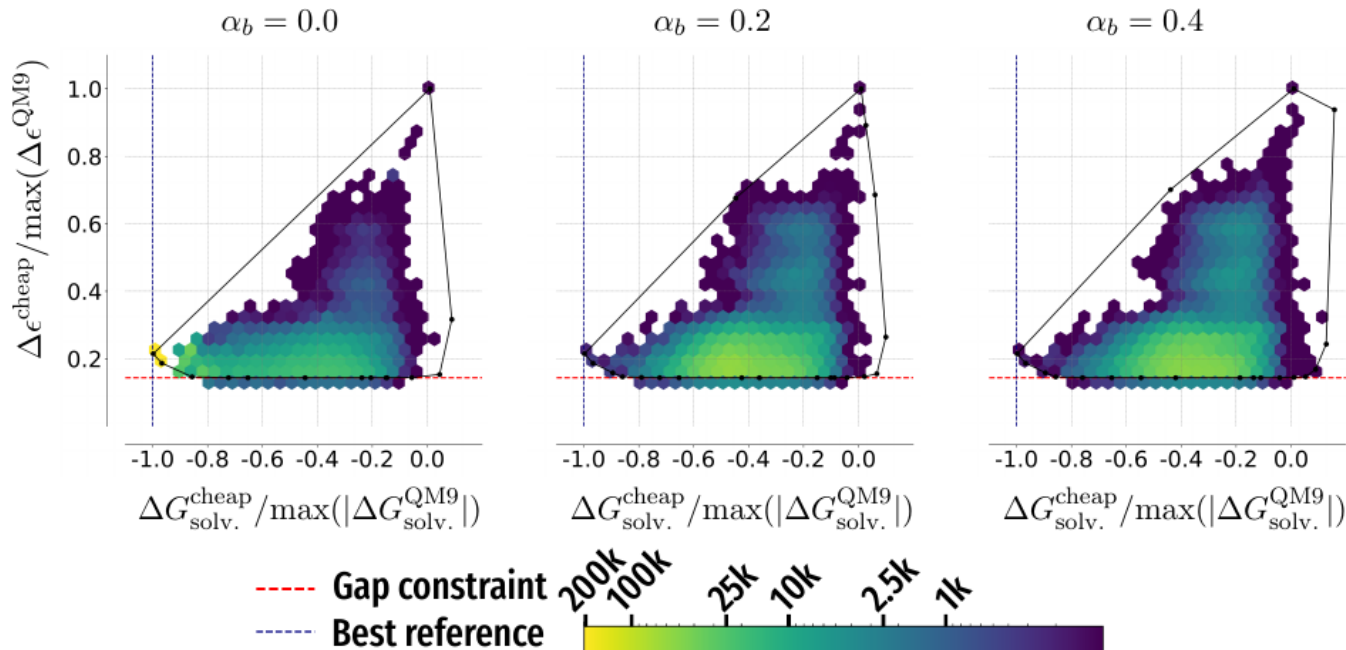


Figure 7: Densities of molecules encountered by example simulations minimizing free energy of solvation  $\Delta G_{\text{solv}}$  with weak HOMO-LUMO gap  $\Delta\epsilon$  constraint in QM9\* for different values of bias proportionality coefficient  $\alpha_b$ .

Table 2: Best and worst EGP\* candidates, data notation is analogous to Table 1. Full list of candidate molecules can be found in Supporting Information.

optimized quantity	$\Delta\epsilon$ constraint	optimized quantity value		relative improvement	
		best	worst	best	worst
$\Delta G_{\text{solv}}$	weak	-1194 $\pm$ 7	-382.2 $\pm$ 1.2	118.0 $\pm$ 0.7	30.84 $\pm$ 0.13
	strong	-269.8 $\pm$ 2.1	-207.6 $\pm$ 0.9	23.19 $\pm$ 0.25	15.65 $\pm$ 0.11
$D$	weak	109.5 $\pm$ 0.9	53.69 $\pm$ 0.12	51.16 $\pm$ 0.48	21.49 $\pm$ 0.07
	strong	59.81 $\pm$ 1.14	25.88 $\pm$ 0.17	34.70 $\pm$ 0.76	11.95 $\pm$ 0.12

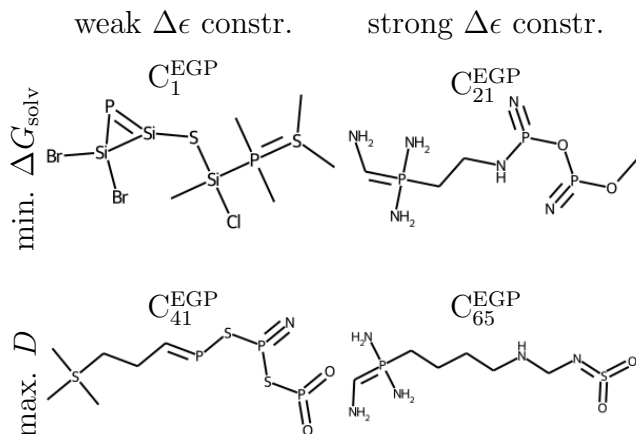


Figure 8: EGP\* candidates that exhibited smallest free energy of solvation  $\Delta G_{\text{solv}}$  or largest dipole  $D$  under weak or strong constraint on the HOMO-LUMO gap  $\Delta\epsilon$ . See the Supporting Information for more information about them.

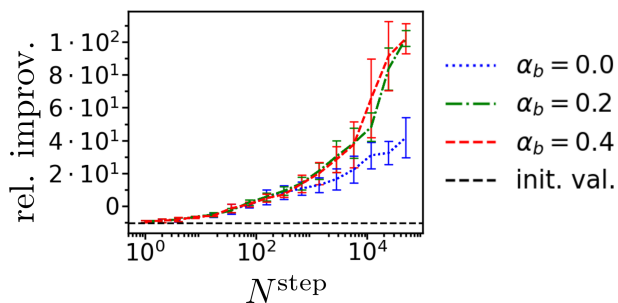


Figure 9: Relative improvement observed at  $N^{\text{step}}$  global Monte Carlo steps for EGP\* simulations optimizing  $\Delta G_{\text{solv}}$  with weak  $\Delta\epsilon$  constraint; results are organized analogously to Figure 6.

rent implementation, it is only feasible to optimize estimates of quantities of interest that can be evaluated with little computational effort due to the large number of evaluations of loss function made during a simulation (see Supporting Information); given successes in using active learning for optimization problems in both configuration<sup>73–76</sup> and chemical<sup>58,77,78</sup> space, our first priority is to combine MOSAiCS with a similar protocol to decrease the number of loss function evaluations done during the simulations. Successful use of Markov Decision Process formalism to accelerate genetic algorithms in chemical space<sup>59</sup> suggests MOSAiCS might similarly be improved with a smarter policy for choosing elementary mutations and crossover moves. On a more general note, any method for generating chemical graphs that can also provide corresponding proposition probability  $P_{\text{prop}}$  needed for  $P_{\text{acc}}$  (4) can be integrated into MOSAiCS framework directly.

While we aimed to propose an approach that would be agnostic to how much is known about the chemical graph set of interest, we still relied on QM9 and EGP to get reasonably rescaled loss functions  $F_{\text{solv}}$  (5) and  $F_{\text{dipole}}$  (6) that were then used during simulations in QM9\* and EGP\*. This dependence on previously published data should become avoidable by implementing more sophisticated schemes<sup>79</sup> for adjusting temperature parameters  $\beta^{(i)}$  based on trajectory history. Also, while we used heavy atoms with connected hydrogens as nodes of chemical graphs to maximize chemical diversity of generated compounds, it is possible to expand the algorithm to using larger compound fragments as nodes instead. If applicable to the optimization problem at hand, this modification should simplify the search by both decreasing effective dimensionality of the graphs considered<sup>26,31</sup> and improving scalability of machine learning models for the molecules of interest.<sup>80,81</sup>

## 5 Code availability

Python implementation of MOSAiCS is available at <https://github.com/chemspacelab/>

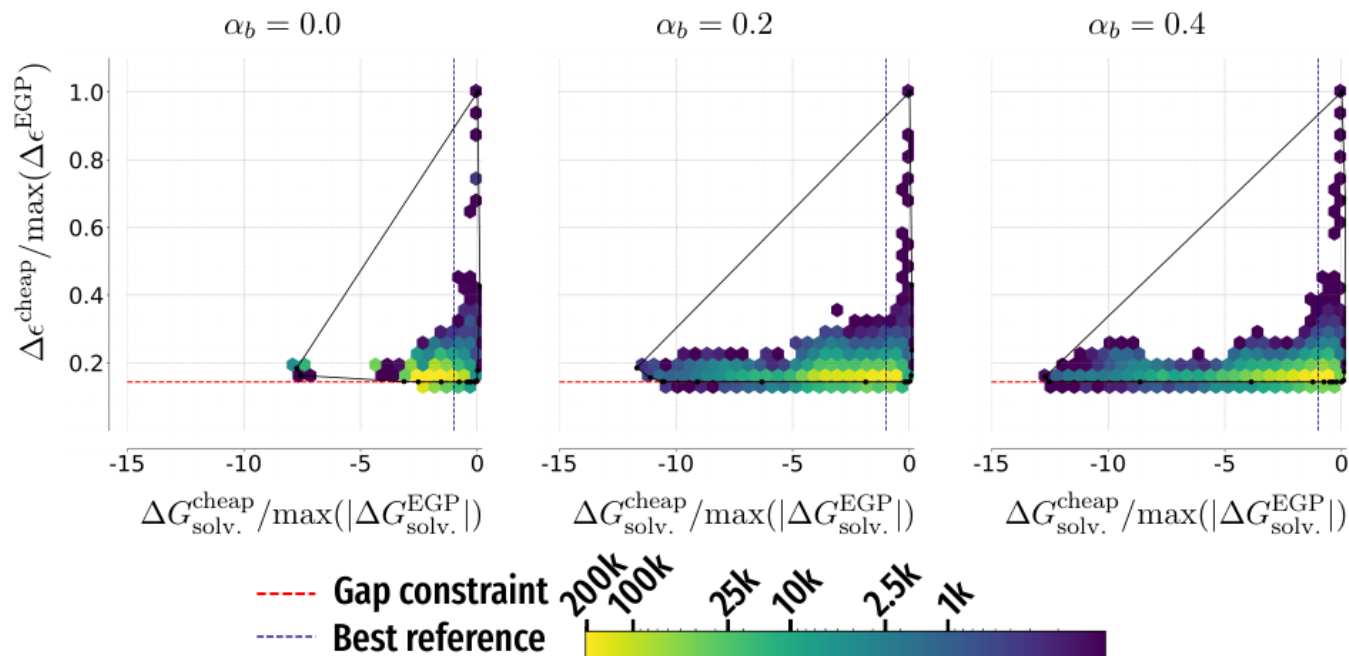


Figure 10: Densities of molecules encountered by simulations minimizing free energy of solvation  $\Delta G_{\text{solv}}$  with weak HOMO-LUMO gap  $\Delta\epsilon$  constraint in EGP\* that produced the candidate with smallest  $\Delta G_{\text{solv}}$  for a given value of bias proportionality coefficient  $\alpha_b$ .

mosaics.

## Supporting Information Available

Details of MOSAiCS implementation and quantity of interest evaluation, discussion of accessibility of QM9\* and EGP\* by our simulations, additional experimental results.

**Acknowledgement** This project has received funding from the European Union’s Horizon 2020 research and innovation programme under grant agreement No 957189 (BIG-MAP) and No 957213 (BATTERY 2030+). O.A.v.L. has received funding from the European Research Council (ERC) under the European Union’s Horizon 2020 research and innovation programme (grant agreement No. 772834). O.A.v.L. has received support as the Ed Clark Chair of Advanced Materials and as a Canada CIFAR AI Chair. O.A.v.L. acknowledges that this research is part of the University of Toronto’s Acceleration Consortium, which receives funding from the Canada First Research Excellence Fund (CFREF). Ob-

taining the presented computational results has been facilitated using the queueing system implemented at <http://leruli.com>. The project has been supported by the Swedish Research Council (Vetenskapsrådet), and the Swedish National Strategic e-Science program eSSSENCE as well as by computing resources from the Swedish National Infrastructure for Computing (SNIC/NAISS).

## References

- (1) Jafari, M.; Botterud, A.; Sakti, A. Decarbonizing power systems: A critical review of the role of energy storage. *Renewable Sustainable Energy Rev.* **2022**, *158*, 112077.
- (2) Korth, M. Large-scale virtual high-throughput screening for the identification of new battery electrolyte solvents: evaluation of electronic structure theory methods. *Phys. Chem. Chem. Phys.* **2014**, *16*, 7919–7926.
- (3) Cheng, L.; Assary, R. S.; Qu, X.; Jain, A.; Ong, S. P.; Rajput, N. N.; Persson, K.;

- Curtiss, L. A. Accelerating Electrolyte Discovery for Energy Storage with High-Throughput Screening. *J. Phys. Chem. Lett.* **2015**, *6*, 283–291.
- (4) Borodin, O.; Olguin, M.; Spear, C. E.; Leiter, K. W.; Knap, J. Towards high throughput screening of electrochemical stability of battery electrolytes. *Nanotechnology* **2015**, *26*, 354003.
  - (5) Qu, X.; Jain, A.; Rajput, N. N.; Cheng, L.; Zhang, Y.; Ong, S. P.; Brafman, M.; Maginn, E.; Curtiss, L. A.; Persson, K. A. The Electrolyte Genome project: A big data approach in battery materials discovery. *Comput. Mater. Sci.* **2015**, *103*, 56–67.
  - (6) Lian, C.; Liu, H.; Li, C.; Wu, J. Hunting ionic liquids with large electrochemical potential windows. *AIChE J.* **2019**, *65*, 804–810.
  - (7) Agarwal, G.; Doan, H. A.; Robertson, L. A.; Zhang, L.; Assary, R. S. Discovery of Energy Storage Molecular Materials Using Quantum Chemistry-Guided Multiobjective Bayesian Optimization. *Chem. Mater.* **2021**, *33*, 8133–8144.
  - (8) Sorkun, E.; Zhang, Q.; Khetan, A.; Sorkun, M. C.; Er, S. RedDB, a computational database of electroactive molecules for aqueous redox flow batteries. *Sci. Data* **2019**, *9*, 718.
  - (9) Huang, B.; von Rudorff, G. F.; von Lilienfeld, O. A. The central role of density functional theory in the AI age. *Science* **2023**, *381*, 170–175.
  - (10) Chang, K. Y. S.; von Lilienfeld, O. A.  $\text{Al}_x\text{Ga}_{1-x}\text{As}$  crystals with direct 2 eV band gaps from computational alchemy. *Phys. Rev. Mater.* **2018**, *2*, 073802.
  - (11) Griego, C. D.; Kitchin, J. R.; Keith, J. A. Acceleration of catalyst discovery with easy, fast, and reproducible computational alchemy. *Int. J. Quantum Chem.* **2021**, *121*, e26380.
  - (12) Eikey, E. A.; Maldonado, A. M.; Griego, C. D.; von Rudorff, G. F.; Keith, J. A. Evaluating quantum alchemy of atoms with thermodynamic cycles: Beyond ground electronic states. *J. Chem. Phys.* **2022**, *156*, 064106.
  - (13) You, J.; Liu, B.; Ying, R.; Pande, V.; Leskovec, J. Graph Convolutional Policy Network for Goal-Directed Molecular Graph Generation. *arXiv* **2018**, 1806.02473.
  - (14) Zhou, Z.; Kearnes, S.; Li, L.; Zare, R. N.; Riley, P. Optimization of Molecules via Deep Reinforcement Learning. *Sci. Rep.* **2019**, *9*, 10752.
  - (15) Ståhl, N.; Falkman, G.; Karlsson, A.; Mathiason, G.; Boström, J. Deep Reinforcement Learning for Multiparameter Optimization in *de novo* Drug Design. *J. Chem. Inf. Model.* **2019**, *59*, 3166–3176.
  - (16) Khemchandani, Y.; O’Hagan, S.; Samanta, S.; Swainston, N.; Roberts, T. J.; Bollegala, D.; Kell, D. B. DeepGraphMolGen, a multi-objective, computational strategy for generating molecules with desirable properties: a graph convolution and reinforcement learning approach. *J. Cheminform.* **2020**, *12*, 53.
  - (17) Horwood, J.; Noutahi, E. Molecular Design in Synthetically Accessible Chemical Space via Deep Reinforcement Learning. *ACS Omega* **2020**, *5*, 32984–32994.
  - (18) Pereira, T.; Abbasi, M.; Ribeiro, B.; Arrais, J. P. Diversity oriented Deep Reinforcement Learning for targeted molecule generation. *J. Cheminform.* **2021**, *13*, 21.
  - (19) Gupta, A.; Müller, A. T.; Huisman, B. J. H.; Fuchs, J. A.; Schneider, P.; Schneider, G. Generative Recurrent Networks for De Novo Drug Design. *Mol. Inform.* **2018**, *37*, 1700111.

- (20) Popova, M.; Shvets, M.; Oliva, J.; Isayev, O. MolecularRNN: Generating realistic molecular graphs with optimized properties. *arXiv* **2019**, 1905.13372.
- (21) Globus, A.; Lawton, J.; Wipke, T. Automatic molecular design using evolutionary techniques. *Nanotechnology* **1999**, *10*, 290.
- (22) Brown, N.; McKay, B.; Gilardoni, F.; Gasteiger, J. A Graph-Based Genetic Algorithm and Its Application to the Multi-objective Evolution of Median Molecules. *J. Chem. Inf. Comput. Sci.* **2004**, *44*, 1079–1087.
- (23) Virshup, A. M.; Contreras-García, J.; Wipf, P.; Yang, W.; Beratan, D. N. Stochastic Voyages into Uncharted Chemical Space Produce a Representative Library of All Possible Drug-Like Compounds. *J. Am. Chem. Soc.* **2013**, *135*, 7296–7303.
- (24) Jensen, J. H. A graph-based genetic algorithm and generative model/Monte Carlo tree search for the exploration of chemical space. *Chem. Sci.* **2019**, *10*, 3567–3572.
- (25) Nigam, A.; Pollice, R.; Aspuru-Guzik, A. Parallel tempered genetic algorithm guided by deep neural networks for inverse molecular design. *Digital Discovery* **2022**, *1*, 390–404.
- (26) Laplaza, R.; Gallarati, S.; Corminboeuf, C. Genetic Optimization of Homogeneous Catalysts. *Chem. Methods* **2022**, *2*, e202100107.
- (27) Gómez-Bombarelli, R.; Wei, J. N.; Duvenaud, D.; Hernández-Lobato, J. M.; Sánchez-Lengeling, B.; Sheberla, D.; Aguilera-Iparraguirre, J.; Hirzel, T. D.; Adams, R. P.; Aspuru-Guzik, A. Automatic Chemical Design Using a Data-Driven Continuous Representation of Molecules. *ACS Cent. Sci.* **2018**, *4*, 268–276.
- (28) Oliveira, A. F.; Da Silva, J. L. F.; Quiles, M. G. Molecular Property Prediction and Molecular Design Using a Supervised Grammar Variational Autoencoder. *J. Chem. Inf. Model.* **2022**, *62*, 817–828.
- (29) Levin, D. A.; Peres, Y. *Markov Chains and Mixing Times: Second Edition*; American Mathematical Society, 2017.
- (30) Fu, T.; Xiao, C.; Li, X.; Glass, L. M.; Sun, J. MIMOSA: Multi-constraint Molecule Sampling for Molecule Optimization. *Proc. Conf. AAAI Artif. Intell.* **2021**, *35*, 125–133.
- (31) Xie, Y.; Shi, C.; Zhou, H.; Yang, Y.; Zhang, W.; Yu, Y.; Lei, L. MARS: Markov Molecular Sampling for Multi-objective Drug Discovery. *arXiv* **2021**, 2103.10432.
- (32) Liang, F.; Wong, W. H. Evolutionary Monte Carlo: applications to C-p model sampling and change point problem. *Stat. Sin.* **2000**, *10*, 317–342.
- (33) Hu, B.; Tsui, K.-W. Distributed evolutionary Monte Carlo for Bayesian computing. *Comput. Stat. Data Anal.* **2010**, *54*, 688–697.
- (34) Spezia, L. Bayesian variable selection in non-homogeneous hidden Markov models through an evolutionary Monte Carlo method. *Comput. Stat. Data Anal.* **2020**, *143*, 106840.
- (35) Hukushima, K.; Nemoto, K. Exchange Monte Carlo Method and Application to Spin Glass Simulations. *J. Phys. Soc. Jpn.* **1996**, *65*, 1604–1608.
- (36) Sambridge, M. A Parallel Tempering algorithm for probabilistic sampling and multimodal optimization. *Geophys. J. Int.* **2014**, *196*, 357–374.
- (37) Angelini, M. C.; Ricci-Tersenghi, F. Monte Carlo algorithms are very effective in finding the largest independent set in sparse random graphs. *Phys. Rev. E* **2019**, *100*, 013302.



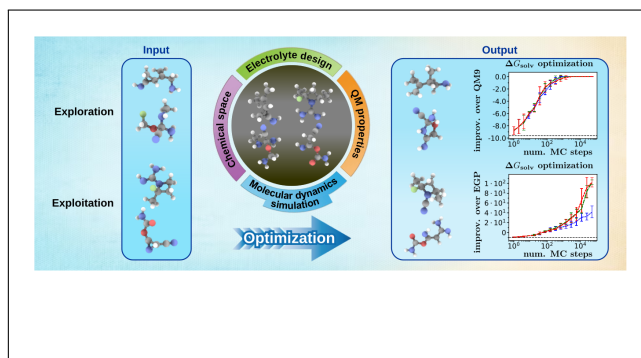
- (38) Holland, J. H. *Adaptation in Natural and Artificial Systems*; University of Michigan Press, Ann Arbor, 1975.
- (39) Jóhannesson, G. H.; Bligaard, T.; Ruban, A. V.; Skriver, H. L.; Jacobsen, K. W.; Nørskov, J. K. Combined Electronic Structure and Evolutionary Search Approach to Materials Design. *Phys. Rev. Lett.* **2002**, *88*, 255506.
- (40) Sharma, S.; Singh, H.; Balint-Kurti, G. G. Genetic algorithm optimization of laser pulses for molecular quantum state excitation. *J. Chem. Phys.* **2010**, *132*, 064108.
- (41) Hastings, W. K. Monte Carlo sampling methods using Markov chains and their applications. *Biometrika* **1970**, *57*, 97–109.
- (42) Iftimie, R.; Salahub, D.; Wei, D.; Schofield, J. Using a classical potential as an efficient importance function for sampling from an ab initio potential. *J. Chem. Phys.* **2000**, *113*, 4852–4862.
- (43) Gelb, L. D. Monte Carlo simulations using sampling from an approximate potential. *J. Chem. Phys.* **2003**, *118*, 7747–7750.
- (44) Jadrich, R. B.; Leiding, J. A. Accelerating Ab Initio Simulation via Nested Monte Carlo and Machine Learned Reference Potentials. *J. Phys. Chem. B* **2020**, *124*, 5488–5497.
- (45) Zhang, L.; Iyyamperumal, R.; Yancey, D. F.; Crooks, R. M.; Henkelman, G. Design of Pt-Shell Nanoparticles with Alloy Cores for the Oxygen Reduction Reaction. *ACS Nano* **2013**, *7*, 9168–9172.
- (46) Anderson, R. M.; Yancey, D. F.; Zhang, L.; Chill, S. T.; Henkelman, G.; Crooks, R. M. A Theoretical and Experimental Approach for Correlating Nanoparticle Structure and Electrocatalytic Activity. *Acc. Chem. Res.* **2015**, *48*, 1351–1357.
- (47) Shields, B. J.; Stevens, J.; Li, J.; Pararam, M.; Damani, F.; Alvarado, J. I. M.; Janey, J. M.; Adams, R. P.; Doyle, A. G. Bayesian reaction optimization as a tool for chemical synthesis. *Nature* **2021**, *590*, 89–96.
- (48) Park, J.; Kim, Y. M.; Hong, S.; Han, B.; Nam, K. T.; Jung, Y. Closed-loop optimization of nanoparticle synthesis enabled by robotics and machine learning. *Matter* **2023**, *6*, 677–690.
- (49) Rahmanian, F.; Flowers, J.; Guevarra, D.; Richter, M.; Fichtner, M.; Donnelly, P.; Gregoire, J. M.; Stein, H. S. Enabling Modular Autonomous Feedback-Loops in Materials Science through Hierarchical Experimental Laboratory Automation and Orchestration. *Adv. Mater. Interfaces* **2022**, *9*, 2101987.
- (50) Stein, H. S.; Sanin, A.; Rahmanian, F.; Zhang, B.; Vogler, M.; Flowers, J. K.; Fischer, L.; Fuchs, S.; Choudhary, N.; Schroeder, L. From materials discovery to system optimization by integrating combinatorial electrochemistry and data science. *Curr. Opin. Electrochem.* **2022**, *35*, 101053.
- (51) Manzano, J. S.; Hou, W.; Zaleskiy, S. S.; Frei, P.; Wang, H.; Kitson, P. J.; Cronin, L. An autonomous portable platform for universal chemical synthesis. *Nat. Chem.* **2022**, *14*, 1311–1318.
- (52) Nigam, A.; Pollice, R.; Krenn, M.; dos Passos Gomes, G.; Aspuru-Guzik, A. Beyond generative models: superfast traversal, optimization, novelty, exploration and discovery (STONED) algorithm for molecules using SELFIES. *Chem. Sci.* **2021**, *12*, 7079–7090.
- (53) Born, J.; Manica, M. Regression Transformer enables concurrent sequence regression and generation for molecular language modelling. *Nat. Mach. Intell.* **2023**, *5*, 432–444.



- (54) Lemm, D.; von Lilienfeld, G. F. v. O. A. Machine learning based energy-free structure predictions of molecules, transition states, and solids. *Nat. Commun.* **2021**, *12*, 4468.
- (55) Weinreich, J.; Lemm, D.; von Rudorff, G. F.; von Lilienfeld, O. Ab initio machine learning of phase space averages. *J. Chem. Phys.* **2022**, *157*, 024303.
- (56) Wang, F.; Landau, D. P. Efficient, Multiple-Range Random Walk Algorithm to Calculate the Density of States. *Phys. Rev. Lett.* **2001**, *86*, 2050–2053.
- (57) Thiede, L. A.; Krenn, M.; Nigam, A. K.; Aspuru-Guzik, A. Curiosity in exploring chemical spaces: intrinsic rewards for molecular reinforcement learning. *Mach. Learn.: Sci. Technol.* **2022**, *3*, 035008.
- (58) Reker, D. Practical considerations for active machine learning in drug discovery. *Drug Discov. Today Technol.* **2019**, *32–33*, 73–79.
- (59) Fu, T.; Gao, W.; Coley, C.; Sun, J. Reinforced Genetic Algorithm for Structure-based Drug Design. *Advances in Neural Information Processing Systems*. 2022; pp 12325–12338.
- (60) Carter, Z. J.; Hollander, K.; Spasov, K. A.; Anderson, K. S.; Jorgensen, W. L. Design, synthesis, and biological testing of biphenylmethyloxazole inhibitors targeting HIV-1 reverse transcriptase. *Bioorg. Med. Chem. Lett.* **2023**, *84*, 129216.
- (61) Borodin, O. Challenges with prediction of battery electrolyte electrochemical stability window and guiding the electrode – electrolyte stabilization. *Curr. Opin. Electrochem.* **2019**, *13*, 86–93.
- (62) Teunissen, J. L.; De Proft, F.; De Vleeschouwer, F. Tuning the HOMO–LUMO Energy Gap of Small Diamondoids Using Inverse Molecular Design. *J. Chem. Theory Comput.* **2017**, *13*, 1351–1365.
- (63) Do HOMO-LUMO Energy Levels and Band Gaps Provide Sufficient Understanding of Dye-Sensitizer Activity Trends for Water Purification? *ACS Omega* **2020**, *5*, 15052–15062.
- (64) Fromer, J. C.; Coley, C. W. Computer-aided multi-objective optimization in small molecule discovery. *Patterns* **2023**, *4*, 100678.
- (65) (a) Halgren, T. A. Merck molecular force field. I. Basis, form, scope, parameterization, and performance of MMFF94. *J. Comput. Chem.* **1996**, *17*, 490–519; (b) Halgren, T. A. Merck molecular force field. II. MMFF94 van der Waals and electrostatic parameters for intermolecular interactions. *J. Comput. Chem.* **1996**, *17*, 520–552; (c) Halgren, T. A. Merck molecular force field. III. Molecular geometries and vibrational frequencies for MMFF94. *J. Comput. Chem.* **1996**, *17*, 553–586; (d) Halgren, T. A.; Nachbar, R. B. Merck molecular force field. IV. Conformational energies and geometries for MMFF94. *J. Comput. Chem.* **1996**, *17*, 587–615; (e) Halgren, T. A. Merck molecular force field. V. Extension of MMFF94 using experimental data, additional computational data, and empirical rules. *J. Comput. Chem.* **1996**, *17*, 616–641; (f) Halgren, T. A. MMFF VI. MMFF94s option for energy minimization studies. *J. Comput. Chem.* **1999**, *20*, 720–729; (g) Halgren, T. A. MMFF VII. Characterization of MMFF94, MMFF94s, and other widely available force fields for conformational energies and for intermolecular-interaction energies and geometries. *J. Comput. Chem.* **1999**, *20*, 730–748.
- (66) Bannwarth, C.; Ehlert, S.; Grimme, S. GFN2-xTB-An Accurate and Broadly Parametrized Self-Consistent Tight-Binding Quantum Chemical Method with Multipole Electrostatics and Density-Dependent Dispersion Contributions.

- J. Chem. Theory Comput.* **2019**, *15*, 1652–1671.
- (67) Ehlert, S.; Stahn, M.; Spicher, S.; Grimme, S. Robust and Efficient Implicit Solvation Model for Fast Semiempirical Methods. *J. Chem. Theory Comput.* **2021**, *17*, 4250–4261.
- (68) (a) Ruddigkeit, L.; van Deursen, R.; Blum, L. C.; Reymond, J.-L. Enumeration of 166 Billion Organic Small Molecules in the Chemical Universe Database GDB-17. *J. Chem. Inf. Model.* **2012**, *52*, 2864–2875; (b) Ramakrishnan, R.; Dral, P. O.; Rupp, M.; von Lilienfeld, O. A. Quantum chemistry structures and properties of 134 kilo molecules. *Sci. Data* **2014**, *1*, 140022.
- (69) Jain, A.; Ong, S. P.; Hautier, G.; Chen, W.; Richards, W. D.; Dacek, S.; Cholia, S.; Gunter, D.; Skinner, D.; Ceder, G.; Persson, K. A. Commentary: The Materials Project: A materials genome approach to accelerating materials innovation. *APL Mater.* **2013**, *1*, 011002.
- (70) Clayden, J.; Greeves, N.; Warren, S. *Organic Chemistry*, 2nd ed.; Oxford University Press, 2012.
- (71) Rathore, N.; Chopra, M.; J. de Pablo, J. Optimal allocation of replicas in parallel tempering simulations. *J. Chem. Phys.* **2005**, *122*, 024111.
- (72) Kone, A.; Kofke, D. A. Selection of temperature intervals for parallel-tempering simulations. *J. Chem. Phys.* **2005**, *122*, 206101.
- (73) Gastegger, M.; Behler, J.; Marquetand, P. Machine learning molecular dynamics for the simulation of infrared spectra. *Chem. Sci.* **2017**, *8*, 6924–6935.
- (74) Podryabinkin, E. V.; Shapeev, A. V. Active learning of linearly parametrized interatomic potentials. *Comput. Mater. Sci.* **2017**, *140*, 171–180.
- (75) Schaaf, L.; Fako, E.; De, S.; Schäfer, A.; Csányi, G. Accurate Reaction Barriers for Catalytic Pathways: An Automatic Training Protocol for Machine Learning Force Fields. *arXiv* **2023**, 2301.09931.
- (76) Vandermause, J.; Xie, Y.; Lim, J. S.; Owen, C. J.; Kozinsky, B. Active learning of reactive Bayesian force fields applied to heterogeneous catalysis dynamics of H/Pt. *Nat. Commun.* **2022**, *13*, 5183.
- (77) Hernández-Lobato, J. M.; Requeima, J.; Pyzer-Knapp, E. O.; Aspuru-Guzik, A. Parallel and Distributed Thompson Sampling for Large-scale Accelerated Exploration of Chemical Space. *arXiv* **2017**, 1706.01825.
- (78) Smith, J. S.; Nebgen, B.; Lubbers, N.; Isayev, O.; Roitberg, A. E. Less is more: Sampling chemical space with active learning. *J. Chem. Phys.* **2018**, *148*, 241733.
- (79) Vouden, W. D.; Farr, W. M.; Mandel, I. Dynamic temperature selection for parallel tempering in Markov chain Monte Carlo simulations. *Mon. Not. R. Astron. Soc.* **2005**, *455*, 1919–1937.
- (80) Huang, B.; von Lilienfeld, O. A. Quantum machine learning using atom-in-molecule-based fragments selected on the fly. *Nat. Chem.* **2020**, *12*, 945–951.
- (81) Huang, B.; von Lilienfeld, O. A.; Krogel, J. T.; Benali, A. Toward DMC Accuracy Across Chemical Space with Scalable  $\Delta$ -QML. *J. Chem. Theory Comput.* **2023**, *19*, 1711–1721.

# TOC Graphic



# Supporting Information:

## Evolutionary Monte Carlo of QM properties in chemical space: Electrolyte design

Konstantin Karandashev,<sup>\*,†</sup> Jan Weinreich,<sup>†</sup> Stefan Heinen,<sup>‡</sup> Daniel Jose Arismendi Arrieta,<sup>¶</sup> Guido Falk von Rudorff,<sup>§,||</sup> Kersti Hermansson,<sup>¶</sup> and O.

Anatole von Lilienfeld<sup>‡,⊥,#</sup>

<sup>†</sup>*University of Vienna, Faculty of Physics, Kolingasse 14-16, AT-1090 Wien, Austria*

<sup>‡</sup>*Vector Institute for Artificial Intelligence, Toronto, ON, M5S 1M1, Canada*

<sup>¶</sup>*Department of Chemistry-Ångström Laboratory, Uppsala University, Box 538, SE-75121 Uppsala, Sweden*

<sup>§</sup>*University Kassel, Department of Chemistry, Heinrich-Plett-Str.40, 34132 Kassel, Germany*

<sup>||</sup>*Center for Interdisciplinary Nanostructure Science and Technology (CINSaT),  
Heinrich-Plett-Straße 40, 34132 Kassel*

<sup>⊥</sup>*Departments of Chemistry, Materials Science and Engineering, and Physics, University of Toronto, St. George Campus, Toronto, ON, Canada*

<sup>#</sup>*Machine Learning Group, Technische Universität Berlin and Institute for the Foundations of Learning and Data, 10587 Berlin, Germany*

E-mail: konstantin.karandashev@univie.ac.at

# 1 Details of elementary mutation and crossover move implementations

While in Subsec. 2.3 of the main text it was convenient to speak about invertible elementary mutations, the corresponding procedures were implemented in terms of *elementary changes* listed in the left column of Table S1, which differ from elementary mutations in treating procedures for creating and destroying nodes separately rather than part of unified mutations changing the number of nodes in a chemical graph. To apply a random mutation to a chemical graph we enumerate all sets of possible elementary change parameters, which is also when we observe constraints on allowed types of covalent bonds and number of nodes. We then randomly choose change parameters among those enumerated, by first choosing the elementary change, and then all other parameters in the order listed in the right column of Table S1. Lastly, we check that straightforward application of the change yields a molecule without nodes with invalid valences and if that is not the case reject the move automatically. The last step’s necessity is illustrated with an example in Figure S1.

In Table S1, whenever we mention choosing a node or a pair of nodes we mean choosing them among a list of all nodes or pairs of nodes such that none of them are equivalent to any other in the chemical graph. This prevents MOSAiCS from considering several mutations that yield the same chemical graph  $X_2$  given an initial chemical graph  $X_1$ , making it straightforward to define the unique inverse change parameters that yield  $X_1$  when applied to  $X_2$ . Enumerating all possible changes for  $X_2$  analogously to  $X_1$  allows straightforward calculation of the proposition probability ratio in acceptance probability expression [Eq. (4) in the main text]. Choosing resonance structure for E2 and E6 is necessary in situations when decreasing bond order, depending on the resonance structure, can yield two distinct molecules corresponding to cases when the changed covalent bond is conserved or broken; such situations are illustrated in Figure S2.

Choosing the parameters of a crossover move starts with assigning the “blue fragments”

Table S1: Elementary changes used in this work along with the corresponding order in which random change parameters were chosen.

Elementary change	Choice order
add node (E1a)	<ol style="list-style-type: none"> <li>1. added node’s heavy atom element</li> <li>2. node to which the new node will be connected with a covalent bond</li> <li>3. order of the new covalent bond</li> </ol>
remove node (E1b)	<ol style="list-style-type: none"> <li>1. removed node’s heavy atom element</li> <li>2. removed node</li> </ol>
change bond order (E2)	<ol style="list-style-type: none"> <li>1. step by which bond order is changed</li> <li>2. altered pair of nodes</li> <li>3. resonance structure</li> </ol>
replace heavy atom (E3)	<ol style="list-style-type: none"> <li>1. node’s new heavy atom element</li> <li>2. changed node</li> </ol>
change valence / change hydrogen number (E4)	<ol style="list-style-type: none"> <li>1. node whose valence is changed</li> <li>2. new number of hydrogens connected to the node</li> </ol>
change valence / add heavy atoms (E5a)	<ol style="list-style-type: none"> <li>1. created nodes’ heavy atom element</li> <li>2. node to which the created nodes will be connected via covalent bonds</li> <li>3. order of the new covalent bonds (also automatically defines the number of added nodes)</li> </ol>
change valence / remove heavy atoms (E5b)	<ol style="list-style-type: none"> <li>1. removed nodes’ heavy atom element</li> <li>2. node whose neighbors will be removed</li> <li>3. order of covalent bonds connecting removed nodes to the molecule (also automatically defines the number of removed nodes)</li> </ol>
change valence / change bond order (E6)	<ol style="list-style-type: none"> <li>1. step by which bond order is changed</li> <li>2. altered pair of nodes</li> <li>3. resonance structure</li> </ol>

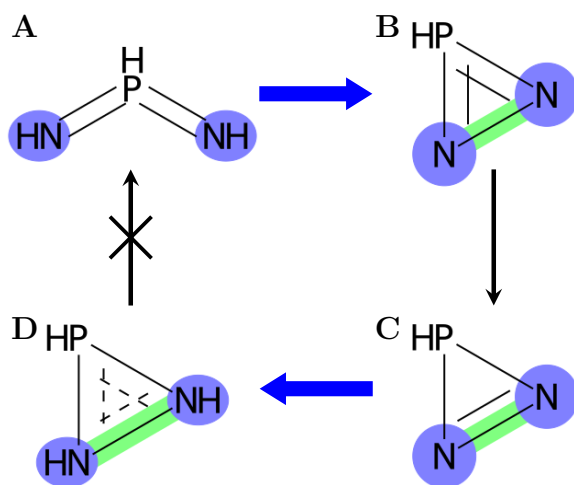
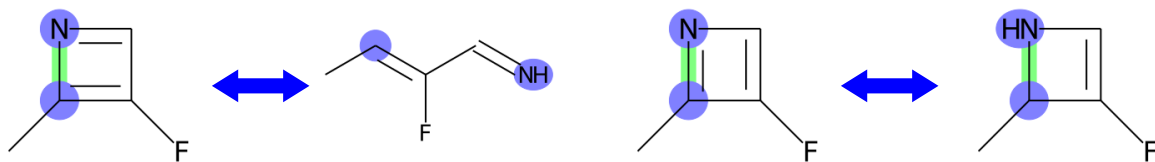


Figure S1: Example of an elementary change that is irreversible due to our definition of valid valence of an atom. Applying elementary change E2 to chemical graph **A** yields chemical graph **B**, which is actually an incorrectly written chemical graph **C**. Applying the inverse of **A**→**B** to **C** yields **D**, which differs from **A**.

(E2)



(E6)

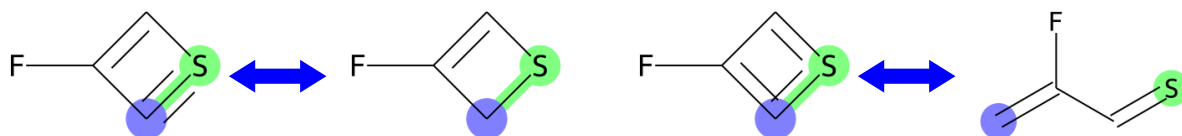


Figure S2: Examples of E2 and E6 elementary changes that decrease order of the covalent bond between the same pairs of nodes by the same values, but yield different results depending on the resonance structure in which the molecules are initialized.

(as illustrated in Figure 4) which are defined as the set of nodes separated by a given number of covalent bonds from an “origin” node. Origin nodes in the two molecules are chosen randomly; then we enumerate all possible blue fragments such that:

- a pair of resonance structures chosen for both molecules allows a one-on-one mapping between green (see Figure 4) covalent bonds of the same order;
- exchanging the blue fragments yields chemical graphs satisfying constraints on the number of nodes in a chemical graph;
- at least one blue fragment and at least one red (see Figure 4) fragment contain more than one node, ensuring that the crossover move is not a simple combination of two E3 elementary changes;
- the number of green bonds is not larger than a certain threshold (set 3 in this work); this is done to limit the number of chemical graph pairs enumerated during the next step.

With the blue fragments chosen we enumerate all pairs of chemical graphs obtained by exchanging them, *i.e.* taking pairs of green bonds from molecules and exchanging nodes between them, thus connecting each molecule’s blue fragment to the red fragment of the other molecule. For each thus generated pair we additionally check that the valences in the exchanged blue and red fragments are valid in the new molecules (to prevent situations analogous to the one illustrated in Figure S1), that none of the newly created green bonds connect the same pair of nodes (to prevent irreversible changes illustrated in Figure S3), and that none of the newly created bonds violate constraints on which types of heavy atoms can be covalently connected.

Of the resulting pairs of chemical graphs one pair, consisting of chemical graphs  $\tilde{X}'$  and  $\tilde{X}''$ , is randomly chosen. The chemical graphs are assigned to replicas  $i'$  and  $i''$  according to the value of sampled probability  $P$  [Eq. (1) in the main text] corresponding to the ordering.



In other words, if both replicas  $i'$  and  $i''$  are greedy the assignment is random; if exactly one is greedy it is assigned the chemical graph corresponding to the smaller value of  $F$ ; if both are exploration replicas the probability of assigning  $\tilde{X}'$  and  $\tilde{X}''$  to replicas  $i'$  and  $i''$  is proportional to

$$P_{\text{order}}(\tilde{X}', \tilde{X}'', i', i'') = \exp \left\{ -\beta^{(i')} \left[ F(\tilde{X}') + V_{\text{bias}}^{(i')}(\tilde{X}') \right] - \beta^{(i'')} \left[ F(\tilde{X}'') + V_{\text{bias}}^{(i'')}(\tilde{X}'') \right] \right\}. \quad (1)$$

Note that if  $i'$  and  $i''$  are a greedy and an exploration replicas and  $F(X^{(i')}) > F(X^{(i'')})$  then the crossover move has no inverse; we avoided such situations by preceding and following a crossover move with attempting a tempering swap move on replicas  $i'$  and  $i''$ . The inverse crossover parameters required to calculate acceptance probability  $P_{\text{acc}}$  [Eq. (4) in the main text] correspond to the same blue fragments being exchanged.

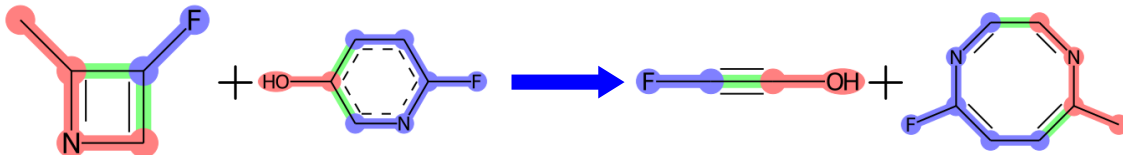


Figure S3: Example of how not checking conservation of number of green bonds during a crossover move results in a non-invertible procedure.

## 2 Experimental details

### 2.1 Estimating quantities of interest

To estimate free energy of solvation  $\Delta G_{\text{solv}}$ , dipole  $D$ , and HOMO-LUMO gap  $\Delta\epsilon$  we used the recipe from Ref. S1, as implemented in the Morfeus package,<sup>S2</sup> to generate the molecule’s conformers and Boltzmann weights  $w_B^{(k)}$  (where  $k$  is conformer index) at  $T = 298.15\text{ K}$  with the MMFF94 forcefield<sup>S3</sup> as implemented<sup>S4</sup> in RDKit.<sup>S5</sup> If converting the lower energy conformer’s geometry back to a chemical graph using the xyz2mol code<sup>S6,S7</sup> proved impossible or yielded a chemical graph different from the initial one we considered conformer generation

to have failed. To decrease the number of conformers considered, we introduced “cut” Boltzmann weights  $\tilde{w}_B^{(k)}$  obtained by solving w.r.t.  $\tilde{w}_B^{(k)}$  and  $\rho_-$

$$\forall k : \tilde{w}_B^{(k)} = \max \left( w_B^{(k)} - \rho_-, 0 \right), \quad (2)$$

$$\frac{\sum_k \tilde{w}_B^{(k)}}{\sum_k w_B^{(k)}} = 1 - \rho_{\text{cut}}, \quad (3)$$

where  $\rho_{\text{cut}}$  is a user-defined parameter. Note that  $\tilde{w}_B^{(k)}$  is exactly zero for higher-energy conformers of the molecule while being a smooth function of  $w_B^{(k)}$ . Then for each conformer with non-zero  $\tilde{w}_B^{(k)}$  we used xtb code<sup>S8</sup> to run GFN2-xTB<sup>S9</sup> calculations with analytical linearized Poisson-Boltzmann (ALPB) model<sup>S10</sup> used to simulate presence of water. For  $D$  and  $\Delta\epsilon$  we took weighted averages of the resulting dipole and HOMO-LUMO gap estimates with  $\tilde{w}_B^{(k)}$  as weights; for  $\Delta G_{\text{solv}}$  the averaged quantity was the difference between GFN2-xTB electronic energies obtained with and without ALPB. Since there is a randomness to generating conformers with Morfeus, the procedure was repeated  $N_{\text{repeat}}$  times with the mean taken as final result and the standard deviation used to estimate the latter’s root mean square error (RMSE). A molecule was considered invalid if one of the  $N_{\text{repeat}}$  generations of MMFF94 coordinates failed or if one of the GFN2-xTB calculations done for the molecule did not converge. This *a priori* limited us to molecules that are not geometrically strained, but we did not consider this restriction important for our end goal applications since geometrically strained molecules are in general less thermodynamically stable, making them less desirable as battery electrolyte components. Lastly, we had to restart some EGP\* simulations due to our code’s failure to handle some xtb code exceptions. Since we encountered such exceptions during less than one in  $10^7$  of evaluation of EGP\* molecules this issue had a negligible impact on the results presented in this work.

The two different sets of calculation parameters mentioned in Subsec. 2.4 of the main text are  $N_{\text{conf}} = 32$  and  $N_{\text{repeat}} = 16$  for “converged,” with  $N_{\text{conf}} = 8$  and  $N_{\text{repeat}} = 1$  for “cheap”;  $\rho_{\text{cut}} = 0.1$  was chosen for both cases. Quantity estimates obtained with the former

exhibited low RMSE’s over QM9 and EGP datasets, but sometimes required relatively large computational time to be calculated, hence the cheap set of parameters were used during our simulations.

Properties of  $\Delta G_{\text{solv}}$ ,  $D$ , and  $\Delta\epsilon$  over molecules in intersections of QM9 with QM9\* and EGP with EGP\* satisfying  $\Delta\epsilon$  constraints are summarized in Table S2. Note that RMSE’s of properties of interest are reasonable over all such molecules. The table also presents reference values used to calculate relative improvements presented in the main text for candidate molecules.

## 2.2 Accessibility of chemical space

To guarantee (at least for  $\alpha_b = 0$  when the sampling is Markovian) that MOSAiCS eventually finds the minimum of loss function over the set of chemical graphs of interest the procedures used to propose trial replica configurations should have *connectivity*, *i.e.* it should be possible to morph each pair of members of the set from one into another using these procedures alone and with only other molecules in this set as intermediates. Mutations M1-M4 are enough to guarantee connectivity in a large variety of relevant sets of chemical graphs, for example those obeying an upper bound on the number of heavy atoms and a constraint on which types of non-carbon heavy atoms can share a covalent bond. Connectivity of this kind of sets is easily seen by “constructing” and “deconstructing” each set member to and from methane. The same argument holds for QM9\* but, unfortunately, not for EGP\* due to P and S atoms being forbidden to share a covalent bond with a hydrogen atom, making it impossible to use mutation M4. Introducing additional mutations M5 and M6 alleviates the problem only partially, with an example of an EGP\* molecule that cannot be transformed to and from methane using elementary mutations presented in Figure S4. This molecule can be considered by the simulations used in this work thanks to crossover moves, but we cannot guarantee this is the case for all such examples. However, we note that all such molecules are geometrically strained, which makes them not interesting for our applications due to

Table S2: Properties of sets of molecules at the intersection of QM9 and QM9\* or EGP and EGP\* that satisfy weak or strong constraint on HOMO-LUMO gap  $\Delta\epsilon$ , namely their number (num. mol.), standard deviations (STD) of optimized quantities (free energy of solvation  $\Delta G_{\text{solv}}$  and dipole  $D$ ) over these molecules, the maximum root mean square errors (RMSEs) observed  $\Delta G_{\text{solv}}$ ,  $D$ , and  $\Delta\epsilon$ , minimum of  $\Delta G_{\text{solv}}$  and maximum of  $D$ , along with SMILES of the molecules for which these extrema values were observed. The total number of molecules (tot. num. mol.) is the number of molecules whose chemical graphs, if extractable from QM9 or EGP coordinates with xyz2mol code, satisfied constraints of QM9\* or EGP\* sets.

$\Delta\epsilon$ constr.	weak	strong
QM9 and QM9* intersection		
tot. num. mol.	89015	-
num. mol.	67826	20325
min. $\Delta G_{\text{solv}}$ , kJ/mol	$(-9.483 \pm 0.007) \cdot 10^1$	$(-5.636 \pm 0.037) \cdot 10^1$
min. $\Delta G_{\text{solv}}$ SMILES	<chem>NC1=NC(=O)N=C(N)N1</chem>	<chem>NC(=O)CCNC(N)=O</chem>
max. RMSE( $\Delta G_{\text{solv}}$ ), kJ/mol	1.807	$6.589 \cdot 10^{-1}$
max. RMSE( $\Delta G_{\text{solv}}$ ) SMILES	<chem>N=C1NC(N)=C(C=O)O1</chem>	<chem>C1C2OC1C21CC1</chem>
STD $\Delta G_{\text{solv}}$ , kJ/mol	9.977	7.100
max. $D$ , debye	$(1.338 \pm 0.000) \cdot 10^1$	$8.532 \pm 0.041$
max. $D$ SMILES	<chem>CN1C=NC(=O)N=C1N</chem>	<chem>O=C1NCCNC(=O)N1</chem>
max. RMSE( $D$ ), debye	$9.450 \cdot 10^{-1}$	$3.325 \cdot 10^{-1}$
max. RMSE( $D$ ) SMILES	<chem>N=C1OCC=C1NC=O</chem>	<chem>C1C2CN3C1C1OC1C23</chem>
STD $D$ , debye	1.831	1.355
max. RMSE( $\Delta\epsilon$ ), eV	1.067	1.067
max. RMSE( $\Delta\epsilon$ ) SMILES	<chem>CCC1CC12C1CC2C1</chem>	<chem>CCC1CC12C1CC2C1</chem>
EGP and EGP* intersection		
tot. num. mol.	9437	-
num. mol.	6190	863
min. $\Delta G_{\text{solv}}$ , kJ/mol	$(-9.474 \pm 0.006) \cdot 10^1$	$(-7.814 \pm 0.019) \cdot 10^1$
min. $\Delta G_{\text{solv}}$ SMILES	<chem>NC1=NC(=O)N=C(N)N1</chem>	<chem>NS(=O)(=O)CCCCCS(N)(=O)=O</chem>
max. RMSE( $\Delta G_{\text{solv}}$ ), kJ/mol	$6.960 \cdot 10^{-1}$	$3.500 \cdot 10^{-1}$
max. RMSE( $\Delta G_{\text{solv}}$ ) SMILES	<chem>N=C1NC=CN1C(N)=O</chem>	<chem>ClCC1CCCCO1</chem>
STD $\Delta G_{\text{solv}}$ , kJ/mol	9.320	8.267
max. $D$ , debye	$(1.326 \pm 0.000) \cdot 10^1$	$8.050 \pm 0.048$
max. $D$ SMILES	<chem>NC1=NC(=O)N=C(N)N1</chem>	<chem>O=S(=O)(F)CCS(=O)(=O)F</chem>
max. RMSE( $D$ ), debye	$6.943 \cdot 10^{-1}$	$3.179 \cdot 10^{-1}$
max. RMSE( $D$ ) SMILES	<chem>N=CNC1=NC=C(N)O1</chem>	<chem>N#CC1CCC(C#N)CC1</chem>
STD $D$ , debye	1.881	1.492
max. RMSE( $\Delta\epsilon$ ), eV	$2.916 \cdot 10^{-1}$	$2.916 \cdot 10^{-1}$
max. RMSE( $\Delta\epsilon$ ) SMILES	<chem>C=C1CC1</chem>	<chem>C=C1CC1</chem>

decreased thermodynamic stability.

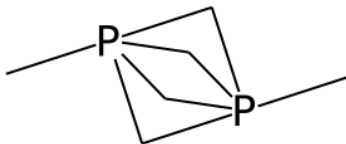


Figure S4: An EGP\* molecule that cannot be transformed to or from methane through EGP\* molecules using elementary mutations alone.

### 3 Additional data obtained during optimization in QM9\* and EGP\*

Full information about QM9\* candidates, including the corresponding values of optimized quantities and how often they were proposed by our simulations, is presented in Table S3; we see that for all optimization problems but for maximizing  $D$  with strong  $\Delta\epsilon$  constraint the agreement between simulations in terms of proposed candidates is close to unanimous. Figure S5 presents QM9\* candidates that were not plotted in Figure 5; while we once again see MOSAiCS’ ability to generate unconventional molecular structures, candidates  $C_7^{\text{QM9}}$ ,  $C_8^{\text{QM9}}$ , and  $C_9^{\text{QM9}}$  demonstrate that our criterion for considering a molecule stable was not always realistic. To compare how fast MOSAiCS found candidates for different optimization problems and  $\alpha_b$  values, we also calculated numbers of chemical graphs considered during a simulation before the candidate was encountered  $N_{\text{req}}^{\text{graph}}$ , total number of chemical graphs considered during a simulation  $N_{\text{tot}}^{\text{graph}}$ , and the number of global steps (as defined in Subsec. 2.5 of the main text) taken by a simulation before the candidate was encountered  $N_{\text{req}}^{\text{step}}$ . For QM9\* simulations mean and standard deviation values of these quantities are summarized in Table S4. Changing the bias proportionality coefficient  $\alpha_b$  did not significantly affect the number of global steps required on average to find a candidate molecule, but did lead to

a more thorough (but also costly) exploration of chemical space, as demonstrated by significant increase of  $\overline{N_{\text{req}}^{\text{graph}}}$  and  $\overline{N_{\text{tot}}^{\text{graph}}}$ . Another interesting observation is that for a given  $\Delta\epsilon$  constraint  $N_{\text{req}}^{\text{step}}$  values are significantly higher for optimization of  $D$  than optimization of  $\Delta G_{\text{solv}}$ . This is likely due to  $\Delta G_{\text{solv}}$  being easier to optimize since free energy of solvation can be accurately decomposed as the sum of scalar contributions from different functional groups in the molecule,<sup>S11</sup> while for the dipole moment such contributions would take vector form whose sum would depend on the groups' placement in Cartesian space. Also note that for all optimization problems but for maximizing  $D$  with a strong  $\Delta\epsilon$  constraint the  $N_{\text{req}}^{\text{step}}$  was typically significantly smaller than the simulation length, which is an indicator of the simulations being converged in these cases. Relative improvement progress plots for optimization problems not shown in the main text are presented in Figure S6; while they look largely analogous to Figure 6, our simulations look less converged for minimization under strong  $\Delta\epsilon$  constraint than under weak  $\Delta\epsilon$  constraint. Plots of densities of QM9\* molecules analogous to Figure 7 are found in Figures S7-S9; analogously to Figure 7 we observe an increase in diversity of considered molecules largely achieved by increasing exploration of chemical space regions less valuable in terms of properties of interest.

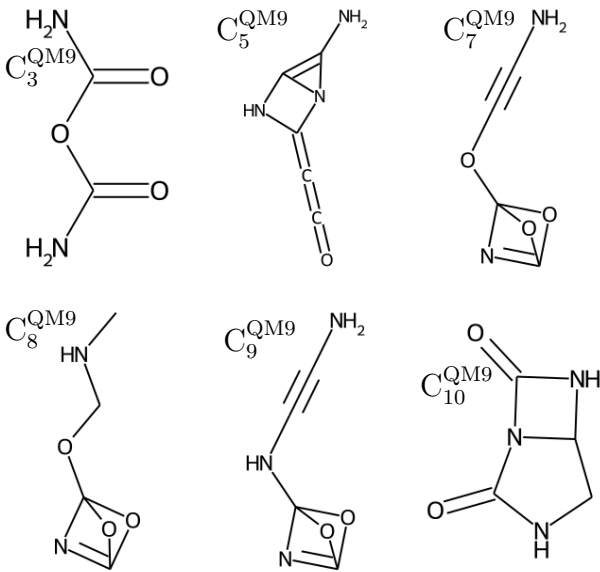


Figure S5: QM9\* candidates that did not exhibit best target property values.

Table S3: QM9\* candidates along with their corresponding optimized quantity values (opt. quant.) and the number of times the molecule was proposed as a candidate by simulations run with different values of the bias proportionality coefficient  $\alpha_b$  (prop. with  $\alpha_b$ ).  $\Delta G_{\text{solv}}$  and  $D$  values are in kJ/mol and debye.

molecule	SMILES	opt. quant.	prop. with $\alpha_b$		
			0.0	0.2	0.4
min. $\Delta G_{\text{solv}}$ (weak $\Delta\epsilon$ constraint)					
$C_1^{\text{QM9}}$	NC1=NC(=O)N=C(N)N1	$(-9.479 \pm 0.006) \cdot 10^1$	8	8	8
min. $\Delta G_{\text{solv}}$ (strong $\Delta\epsilon$ constraint)					
$C_2^{\text{QM9}}$	NC(=O)NCNC(N)=O	$(-6.819 \pm 0.060) \cdot 10^1$	7	8	8
$C_3^{\text{QM9}}$	NC(=O)OC(N)=O	$(-6.727 \pm 0.000) \cdot 10^1$	1	0	0
max. $D$ (weak $\Delta\epsilon$ constraint)					
$C_4^{\text{QM9}}$	NC1=C2OC(=CC=O)N12	$(1.573 \pm 0.010) \cdot 10^1$	8	7	8
$C_5^{\text{QM9}}$	NC1=C2NC(=C=C=O)N12	$(1.523 \pm 0.000) \cdot 10^1$	0	1	0
max. $D$ (strong $\Delta\epsilon$ constraint)					
$C_6^{\text{QM9}}$	FC(F)=C=C=C1OCO1	$(1.114 \pm 0.000) \cdot 10^1$	1	4	1
$C_7^{\text{QM9}}$	NC#COC12N=C(O1)O2	$(1.083 \pm 0.003) \cdot 10^1$	4	2	2
$C_8^{\text{QM9}}$	CNCO12N=C(O1)O2	$(1.051 \pm 0.020) \cdot 10^1$	0	1	4
$C_9^{\text{QM9}}$	NC#CNC12N=C(O1)O2	$(1.036 \pm 0.007) \cdot 10^1$	1	1	1
$C_{10}^{\text{QM9}}$	O=C1NCC2NC(=O)N12	$(1.000 \pm 0.000) \cdot 10^1$	2	0	0

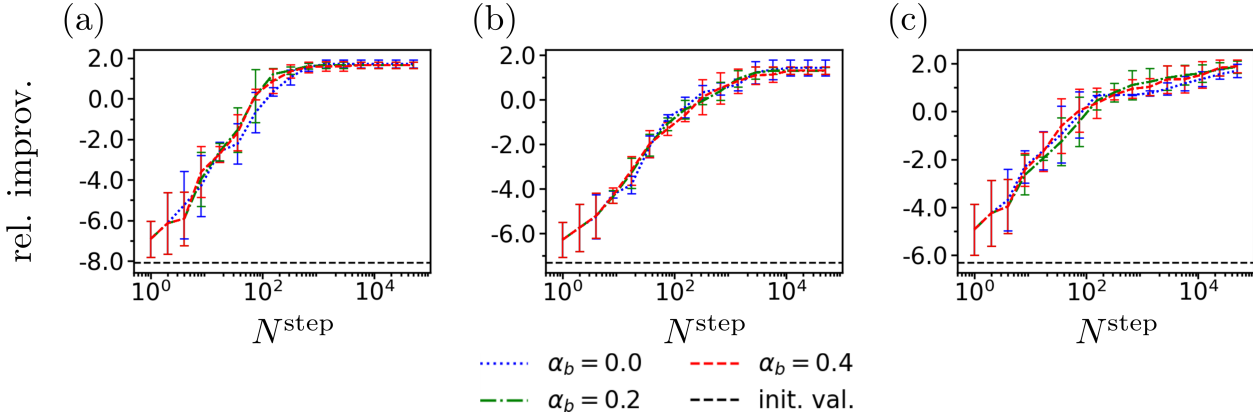


Figure S6: Relative improvement (as defined in Sec. 3 of the main text and estimated from  $\Delta G_{\text{solv}}^{\text{cheap}}$  or  $D^{\text{cheap}}$ ) observed at  $N^{\text{step}}$  global Monte Carlo steps for QM9\* simulations optimizing (a)  $D$  with weak  $\Delta\epsilon$  constraint, (b)  $\Delta G_{\text{solv}}$  with strong  $\Delta\epsilon$  constraint, and (c)  $D$  with strong  $\Delta\epsilon$  constraint. For each value of the biasing potential  $\alpha_b$  we plot the mean value over different random generator seeds, the error bars corresponding to standard deviation. "init. val." is the relative improvement of the simulations' starting molecule, *i.e.* methane.

Table S4: Mean and standard deviation of number of chemical graphs considered by a simulation before its candidate was encountered [ $\overline{N_{\text{req}}^{\text{graph}}}$  and  $\sigma(N_{\text{req}}^{\text{graph}})$ ], total number of chemical graphs considered by a simulation [ $\overline{N_{\text{tot}}^{\text{graph}}}$  and  $\sigma(N_{\text{tot}}^{\text{graph}})$ ], and number of global steps taken by a simulation before the candidate was encountered [ $\overline{N_{\text{req}}^{\text{step}}}$  and  $\sigma(N_{\text{req}}^{\text{step}})$ ] observed for trajectories in QM9\* for different optimization problems (minimize free energy of solvation  $\Delta G_{\text{solv}}$  or maximize dipole  $D$  under weak or strong constraint on HOMO-LUMO gap  $\Delta\epsilon$ ) and different values of the bias proportionality coefficient  $\alpha_b$ .

$\Delta\epsilon$ constr.	weak			strong		
$\alpha_b$	0.0	0.2	0.4	0.0	0.2	0.4
min. $\Delta G_{\text{solv}}$						
$\overline{N_{\text{req}}^{\text{graph}}}$	$4.072 \cdot 10^3$	$5.164 \cdot 10^3$	$1.449 \cdot 10^4$	$3.854 \cdot 10^3$	$8.391 \cdot 10^3$	$8.544 \cdot 10^3$
$\sigma(N_{\text{req}}^{\text{graph}})$	$1.672 \cdot 10^3$	$2.979 \cdot 10^3$	$1.053 \cdot 10^4$	$2.347 \cdot 10^3$	$4.339 \cdot 10^3$	$6.707 \cdot 10^3$
$\overline{N_{\text{tot}}^{\text{graph}}}$	$2.352 \cdot 10^5$	$6.229 \cdot 10^5$	$6.862 \cdot 10^5$	$1.394 \cdot 10^5$	$4.304 \cdot 10^5$	$4.559 \cdot 10^5$
$\sigma(N_{\text{tot}}^{\text{graph}})$	$3.447 \cdot 10^3$	$1.588 \cdot 10^3$	$2.171 \cdot 10^3$	$3.188 \cdot 10^3$	$1.395 \cdot 10^3$	$1.677 \cdot 10^3$
$\overline{N_{\text{req}}^{\text{step}}}$	$4.234 \cdot 10^2$	$3.231 \cdot 10^2$	$7.781 \cdot 10^2$	$6.704 \cdot 10^2$	$5.584 \cdot 10^2$	$5.181 \cdot 10^2$
$\sigma(N_{\text{req}}^{\text{step}})$	$1.786 \cdot 10^2$	$1.823 \cdot 10^2$	$5.627 \cdot 10^2$	$3.729 \cdot 10^2$	$2.785 \cdot 10^2$	$4.025 \cdot 10^2$
max. $D$						
$\overline{N_{\text{req}}^{\text{graph}}}$	$2.126 \cdot 10^4$	$3.131 \cdot 10^4$	$5.182 \cdot 10^4$	$1.164 \cdot 10^5$	$2.290 \cdot 10^5$	$2.181 \cdot 10^5$
$\sigma(N_{\text{req}}^{\text{graph}})$	$1.589 \cdot 10^4$	$1.762 \cdot 10^4$	$4.687 \cdot 10^4$	$3.757 \cdot 10^4$	$1.424 \cdot 10^5$	$1.285 \cdot 10^5$
$\overline{N_{\text{tot}}^{\text{graph}}}$	$2.426 \cdot 10^5$	$6.591 \cdot 10^5$	$7.169 \cdot 10^5$	$2.022 \cdot 10^5$	$4.765 \cdot 10^5$	$4.842 \cdot 10^5$
$\sigma(N_{\text{tot}}^{\text{graph}})$	$4.052 \cdot 10^3$	$9.418 \cdot 10^2$	$1.312 \cdot 10^3$	$7.042 \cdot 10^3$	$1.593 \cdot 10^3$	$1.150 \cdot 10^3$
$\overline{N_{\text{req}}^{\text{step}}}$	$2.779 \cdot 10^3$	$1.896 \cdot 10^3$	$2.886 \cdot 10^3$	$2.482 \cdot 10^4$	$2.063 \cdot 10^4$	$1.851 \cdot 10^4$
$\sigma(N_{\text{req}}^{\text{step}})$	$2.357 \cdot 10^3$	$1.099 \cdot 10^3$	$2.661 \cdot 10^3$	$9.271 \cdot 10^3$	$1.474 \cdot 10^4$	$1.314 \cdot 10^4$



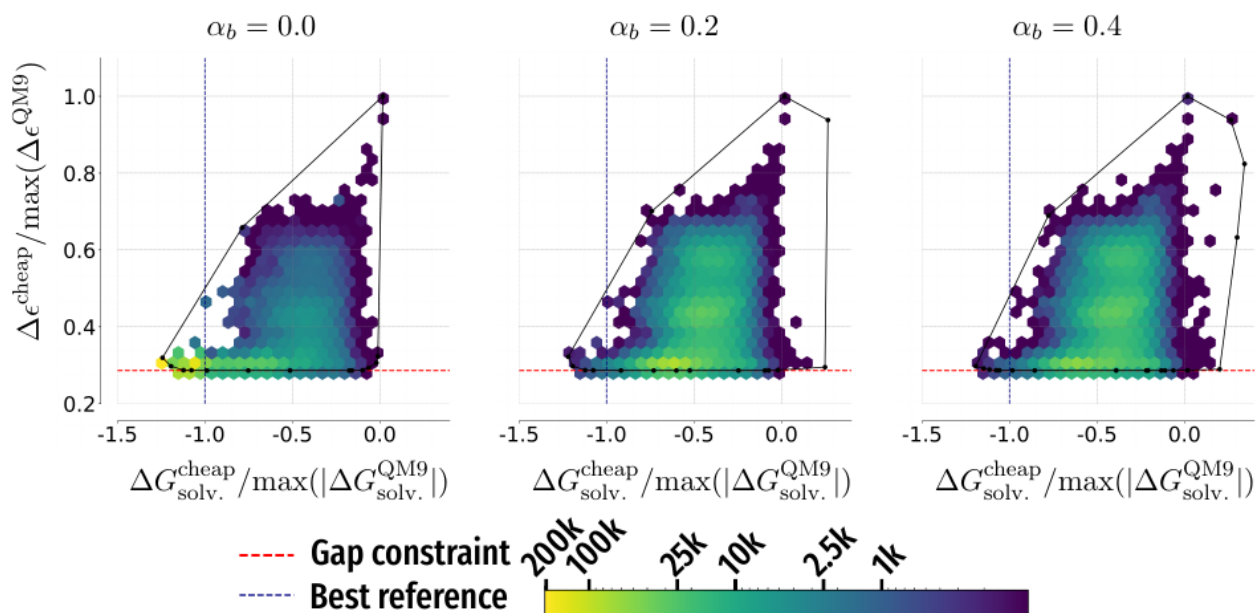


Figure S7: Densities of molecules encountered by example simulations minimizing free energy of solvation  $\Delta G_{\text{solv}}$  with strong HOMO-LUMO gap  $\Delta\epsilon$  constraint in QM9\* that produced the candidate with smallest  $\Delta G_{\text{solv}}$  for a given value of bias proportionality coefficient  $\alpha_b$ .

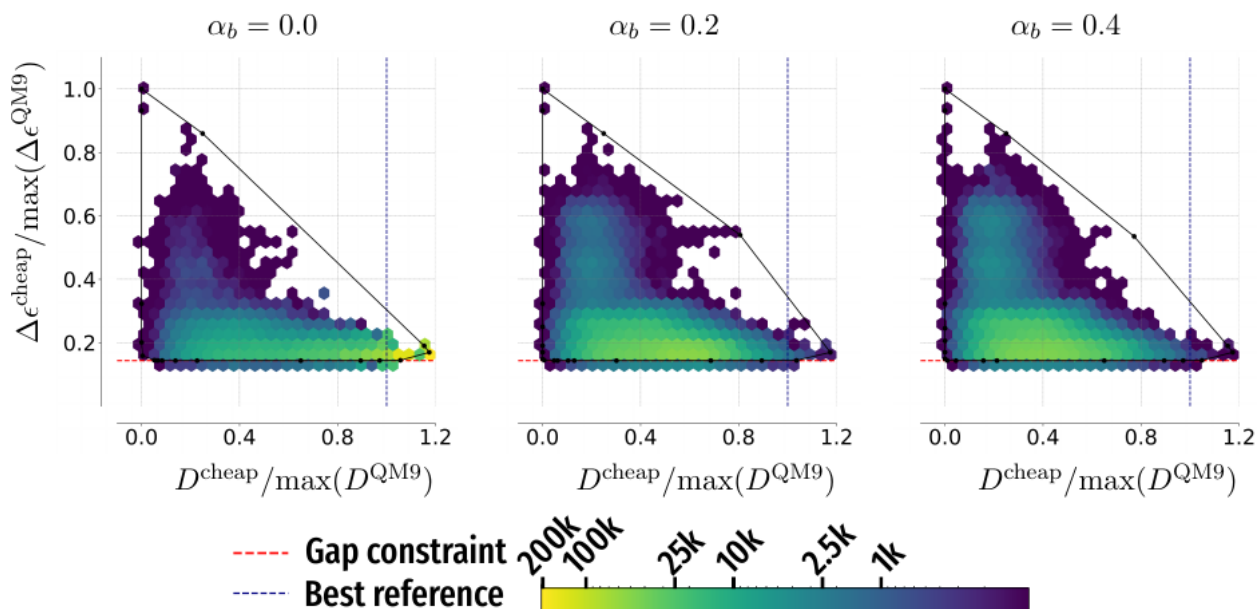


Figure S8: Densities of molecules encountered by example simulations maximizing dipole  $D$  with weak HOMO-LUMO gap  $\Delta\epsilon$  constraint in QM9\* that produced the candidate with largest  $D$  for a given value of bias proportionality coefficient  $\alpha_b$ .

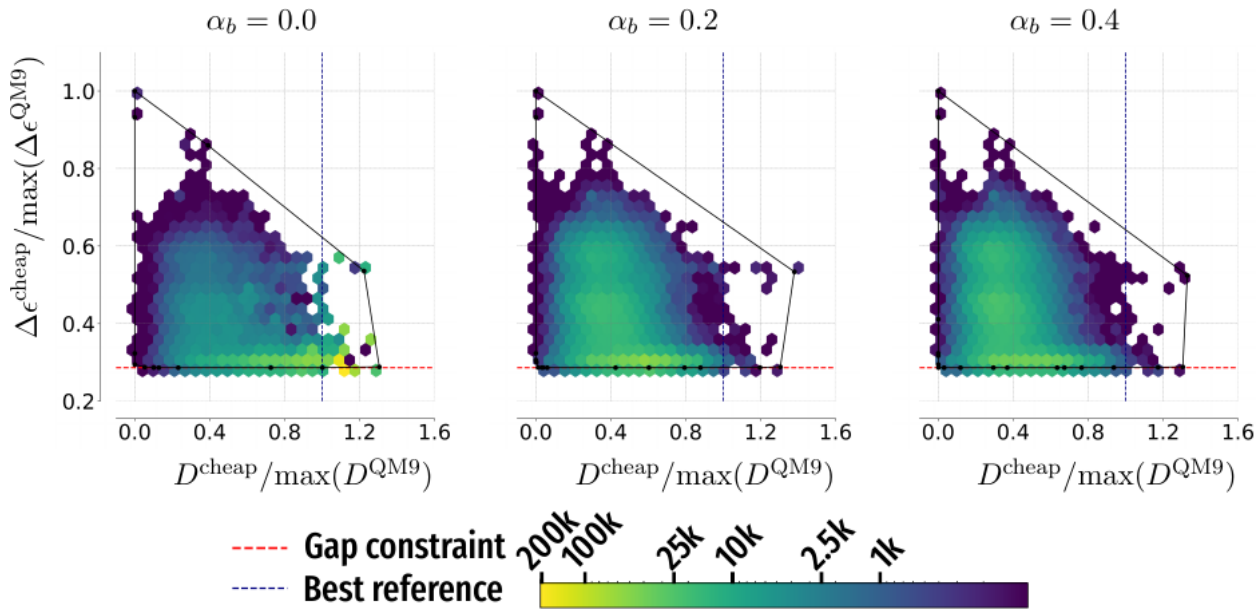


Figure S9: Densities of molecules encountered by example simulations maximizing dipole  $D$  with strong HOMO-LUMO gap  $\Delta\epsilon$  constraint in QM9\* that produced the candidate with largest  $D$  for a given value of bias proportionality coefficient  $\alpha_b$ .

Due to the large number of candidates found in EGP\* their full lists are left for Subsec. 3.2. We summarize how well these molecules were optimized for different optimization problems and  $\alpha_b$  values in Table S5; we observe from the behavior of average optimized property values of candidates  $\overline{D^{\text{best}}}$  and  $\overline{\Delta G_{\text{solv}}^{\text{best}}}$  that adding biasing potential at worst did not significantly affect optimization results and at best provided significant improvements. Table S5 summarizes the behavior of  $N_{\text{req}}^{\text{graph}}$ ,  $N_{\text{tot}}^{\text{graph}}$ , and  $N_{\text{req}}^{\text{step}}$  for our EGP\* simulations. Increasing  $\alpha_b$  consistently increased the number of molecules explored by a trajectory; the  $N_{\text{req}}^{\text{step}}$  values comparable to the total simulation length is an indicator of these simulations not being converged. Analogously to Figure 9, Figure S10 shows how using non-zero  $\alpha_b$  could accelerate finding better candidates w.r.t the number of global Monte Carlo steps. However, we need to underline that, as indicated by  $N_{\text{req}}^{\text{graph}}$  and  $N_{\text{tot}}^{\text{graph}}$  values in Table S5, a non-zero  $\alpha_b$  actually increased the computational time spent on proposing a candidate since MOSAiCS considered more chemical graphs during the corresponding simulations. Plots of densities of EGP\* molecules analogous to Figure 10 are found in Figures S11-S13; analogously to Figure 10 we observe that increasing  $\alpha_b$  tended to help the simulations explore

regions of chemical space more valuable in terms of optimized quantities.

Table S5: Numbers of chemical graphs considered by a trajectory before the candidate molecule was encountered  $N_{\text{req}}^{\text{graph}}$ , total numbers of chemical graphs considered by a trajectory  $N_{\text{tot}}^{\text{graph}}$ , and numbers of global steps after which the candidate was encountered [ $N_{\text{req}}^{\text{step}}$  and  $\sigma(N_{\text{req}}^{\text{step}})$ ] observed for EGP\* simulations; results are labeled analogously to Table S4.

$\Delta\epsilon$ constr.	weak			strong		
$\alpha_b$	0.0	0.2	0.4	0.0	0.2	0.4
min. $\Delta G_{\text{solv}}$						
$N_{\text{req}}^{\text{graph}}$	$1.533 \cdot 10^5$	$5.509 \cdot 10^5$	$4.916 \cdot 10^5$	$2.518 \cdot 10^5$	$4.992 \cdot 10^5$	$4.442 \cdot 10^5$
$\sigma(N_{\text{req}}^{\text{graph}})$	$3.857 \cdot 10^4$	$1.428 \cdot 10^5$	$1.658 \cdot 10^5$	$3.899 \cdot 10^4$	$2.052 \cdot 10^5$	$2.479 \cdot 10^5$
$N_{\text{tot}}^{\text{graph}}$	$1.824 \cdot 10^5$	$6.895 \cdot 10^5$	$7.736 \cdot 10^5$	$3.085 \cdot 10^5$	$7.555 \cdot 10^5$	$8.969 \cdot 10^5$
$\sigma(N_{\text{tot}}^{\text{graph}})$	$1.236 \cdot 10^4$	$8.907 \cdot 10^3$	$6.908 \cdot 10^3$	$1.047 \cdot 10^4$	$6.802 \cdot 10^3$	$4.660 \cdot 10^3$
$N_{\text{req}}^{\text{step}}$	$3.841 \cdot 10^4$	$3.963 \cdot 10^4$	$3.119 \cdot 10^4$	$3.777 \cdot 10^4$	$3.228 \cdot 10^4$	$2.428 \cdot 10^4$
$\sigma(N_{\text{req}}^{\text{step}})$	$1.174 \cdot 10^4$	$1.091 \cdot 10^4$	$1.095 \cdot 10^4$	$7.706 \cdot 10^3$	$1.406 \cdot 10^4$	$1.399 \cdot 10^4$
max. $D$						
$N_{\text{req}}^{\text{graph}}$	$2.141 \cdot 10^5$	$5.646 \cdot 10^5$	$6.574 \cdot 10^5$	$2.759 \cdot 10^5$	$5.532 \cdot 10^5$	$5.779 \cdot 10^5$
$\sigma(N_{\text{req}}^{\text{graph}})$	$2.881 \cdot 10^4$	$1.192 \cdot 10^5$	$7.904 \cdot 10^4$	$3.755 \cdot 10^4$	$1.794 \cdot 10^5$	$2.566 \cdot 10^5$
$N_{\text{tot}}^{\text{graph}}$	$2.537 \cdot 10^5$	$7.740 \cdot 10^5$	$8.427 \cdot 10^5$	$3.269 \cdot 10^5$	$8.604 \cdot 10^5$	$9.540 \cdot 10^5$
$\sigma(N_{\text{tot}}^{\text{graph}})$	$1.296 \cdot 10^4$	$1.401 \cdot 10^4$	$1.016 \cdot 10^4$	$1.532 \cdot 10^4$	$7.360 \cdot 10^3$	$2.848 \cdot 10^3$
$N_{\text{req}}^{\text{step}}$	$3.905 \cdot 10^4$	$3.617 \cdot 10^4$	$3.882 \cdot 10^4$	$4.033 \cdot 10^4$	$3.150 \cdot 10^4$	$3.001 \cdot 10^4$
$\sigma(N_{\text{req}}^{\text{step}})$	$6.732 \cdot 10^3$	$8.028 \cdot 10^3$	$4.668 \cdot 10^3$	$5.221 \cdot 10^3$	$1.073 \cdot 10^4$	$1.360 \cdot 10^4$

Lastly, the difference between cheap and converged estimates of  $D$  and  $\Delta G_{\text{solv}}$  is very small for rigid molecules that only have one local minimum in configuration space (*e.g.* benzene), but it can become significant for larger non-rigid molecules with many valid conformers. To compare how much this difference affected candidate molecules obtained in this work we introduced “numerical error measure”  $\Delta_{\text{cheap}}^{\text{conv}}$  defined as the ratio of mean absolute error of the cheap estimate relative to the converged one divided by standard deviation of the converged estimate over the pre-final (as defined in Subsec. 2.5 of the main text) molecules. Its values for QM9\* and EGP\* simulations are presented in Table S6. For QM9\*, we note that maximizing  $D$  under strong  $\Delta\epsilon$  constraint was apparently much more affected by using  $D^{\text{cheap}}$  in the minimization function, which may be the reason simulations for that optimiza-

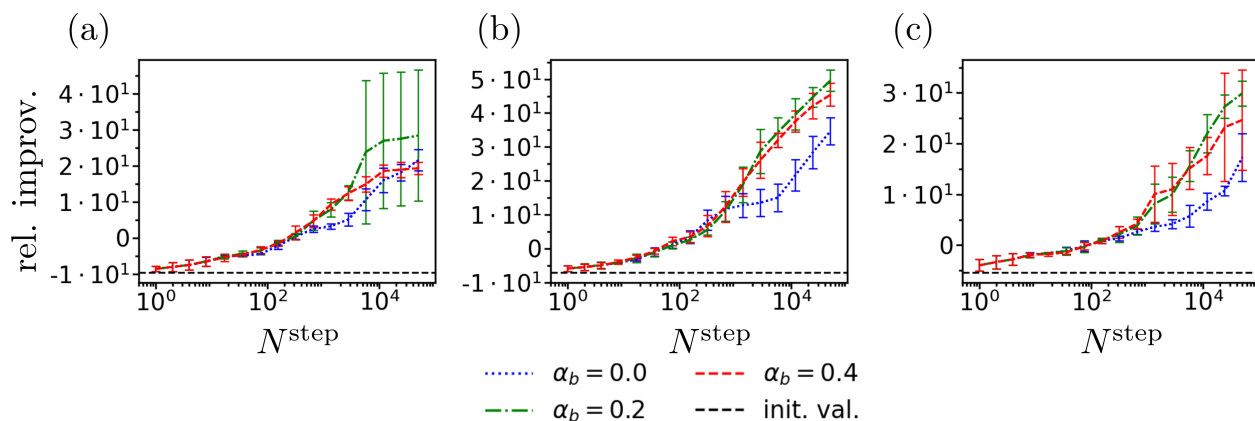


Figure S10: Relative improvement observed at  $N^{\text{step}}$  global Monte Carlo steps for EGP\* simulations optimizing (a)  $D$  with weak  $\Delta\epsilon$  constraint, (b)  $\Delta G_{\text{solv}}$  with strong  $\Delta\epsilon$  constraint, and (c)  $D$  with strong  $\Delta\epsilon$  constraint. Results are organized analogously to Figure S6.

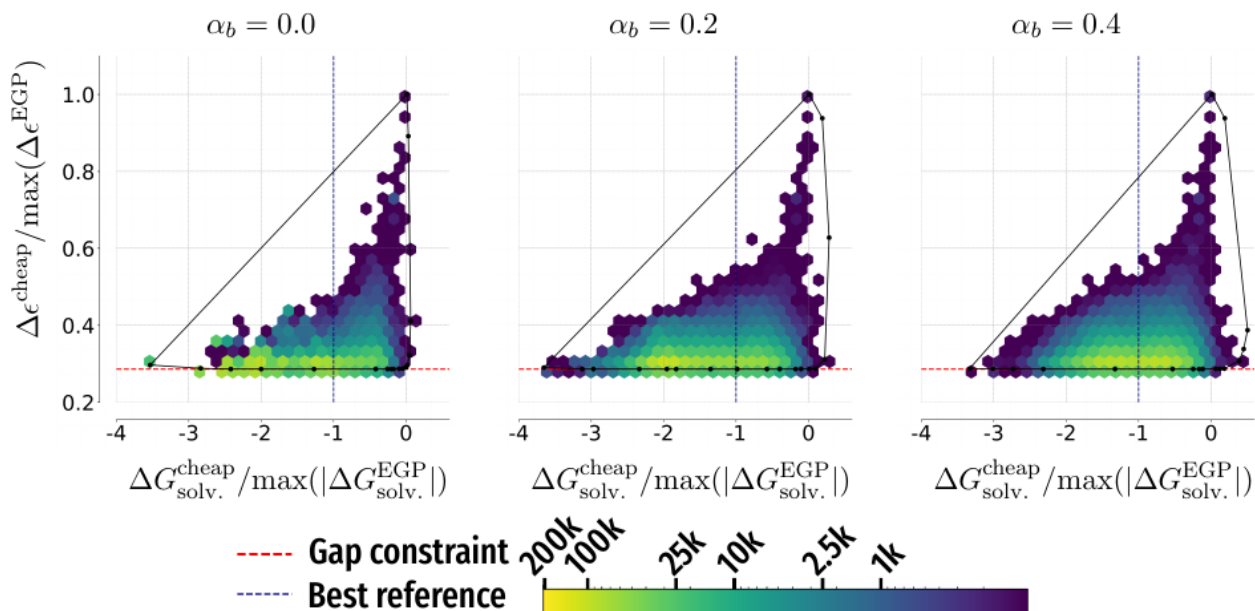


Figure S11: Densities of molecules encountered by simulations minimizing free energy of solvation  $\Delta G_{\text{solv}}$  with strong HOMO-LUMO gap  $\Delta\epsilon$  constraint in EGP\* that produced the candidate with smallest  $\Delta G_{\text{solv}}$  for a given value of bias proportionality coefficient  $\alpha_b$ .

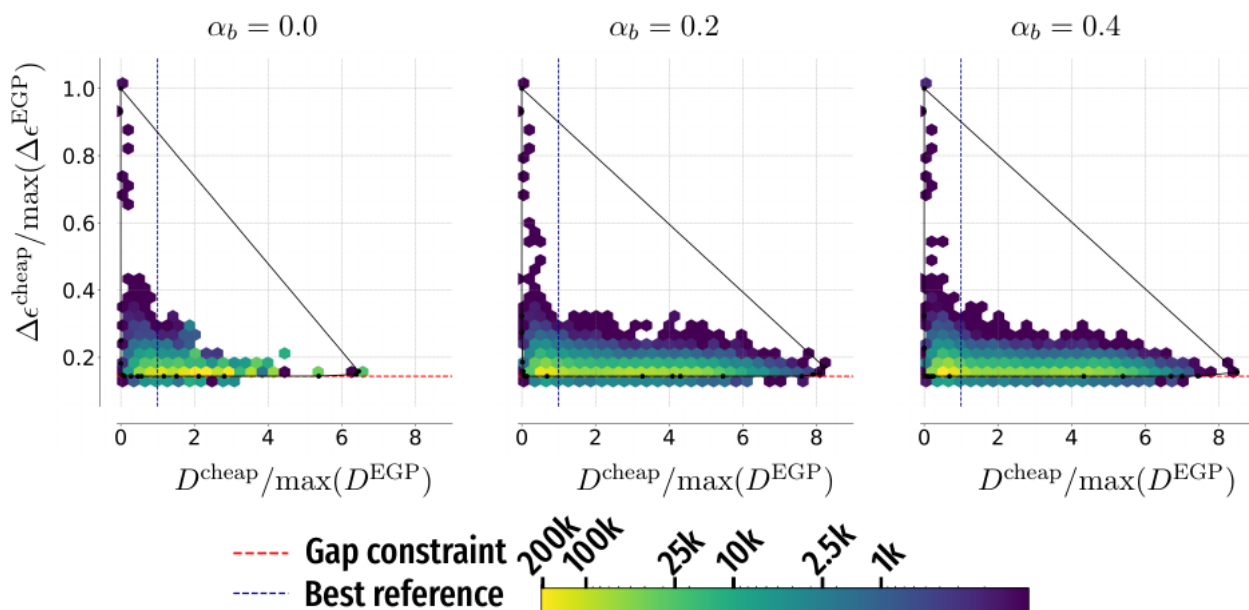


Figure S12: Densities of molecules encountered by simulations maximizing dipole  $D$  with weak HOMO-LUMO gap  $\Delta\epsilon$  constraint in EGP\* that produced the candidate with largest  $D$  for a given value of bias proportionality coefficient  $\alpha_b$ .

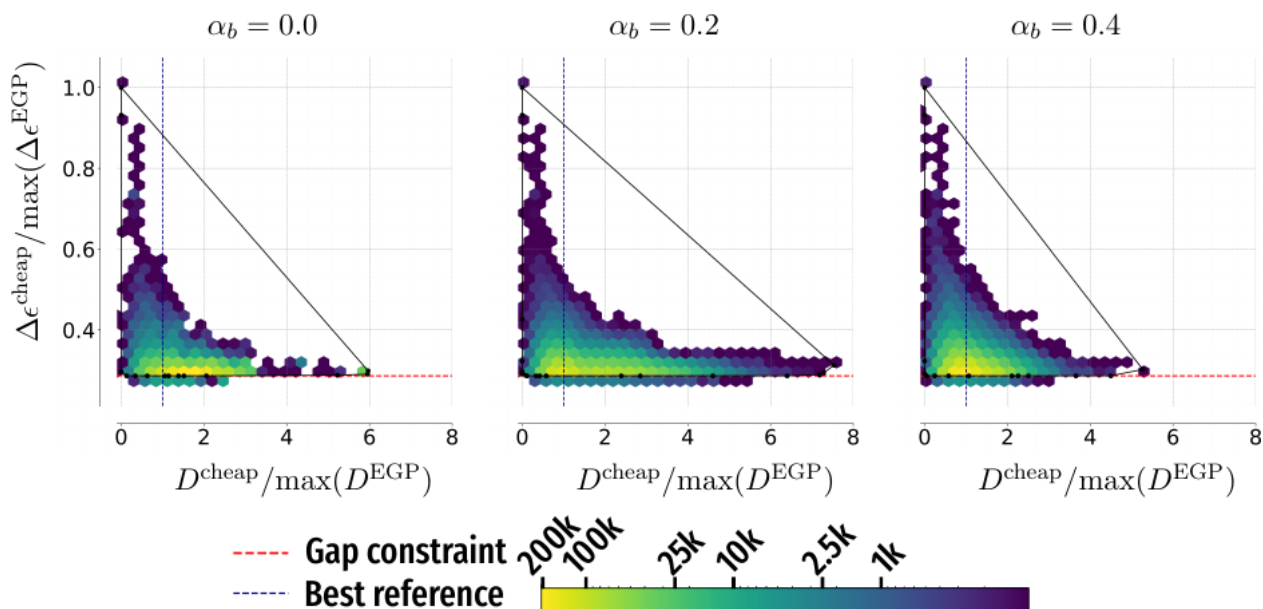


Figure S13: Densities of molecules encountered by simulations maximizing dipole  $D$  with strong HOMO-LUMO gap  $\Delta\epsilon$  constraint in EGP\* that produced the candidate with largest  $D$  for a given value of bias proportionality coefficient  $\alpha_b$ .

tion problem agreed on candidate molecules much less frequently than for the other three. We also observe that for a given optimization problem simulations in EGP\* were much more affected by cheap/converged difference than the ones in QM9\*, likely due to EGP\* consisting of larger molecules with more conformers to be accounted for. This added to EGP\* being the more challenging set of molecules to search through compared to QM9\*.

Table S6: Measure of error caused by using cheap version of optimized quantity during the simulation  $\Delta_{\text{cheap}}^{\text{conv}}$  (see Sec. 3 for definition) observed during simulations in QM9\* or EGP\*, while maximizing dipole  $D$  or minimizing free energy of solvation  $\Delta G_{\text{solv}}$ , under a weak or strong constraint on the HOMO-LUMO gap  $\Delta\epsilon$ , and with different values of the bias proportionality coefficient  $\alpha_b$ .

Optimization problem	$\Delta_{\text{cheap}}^{\text{conv}}$		
	$\alpha_b = 0.0$	$\alpha_b = 0.2$	$\alpha_b = 0.4$
QM9*			
min. $\Delta G_{\text{solv}}$ (weak $\Delta\epsilon$ constraint)	$2.009 \cdot 10^{-1}$	$2.013 \cdot 10^{-1}$	$2.010 \cdot 10^{-1}$
min. $\Delta G_{\text{solv}}$ (strong $\Delta\epsilon$ constraint)	$1.827 \cdot 10^{-1}$	$1.814 \cdot 10^{-1}$	$1.834 \cdot 10^{-1}$
max. $D$ (weak $\Delta\epsilon$ constraint)	$2.635 \cdot 10^{-1}$	$2.658 \cdot 10^{-1}$	$2.714 \cdot 10^{-1}$
max. $D$ (strong $\Delta\epsilon$ constraint)	$4.108 \cdot 10^{-1}$	$4.189 \cdot 10^{-1}$	$4.270 \cdot 10^{-1}$
EGP*			
min. $\Delta G_{\text{solv}}$ (weak $\Delta\epsilon$ constraint)	$2.889 \cdot 10^{-1}$	$8.493 \cdot 10^{-1}$	$7.993 \cdot 10^{-1}$
min. $\Delta G_{\text{solv}}$ (strong $\Delta\epsilon$ constraint)	$4.145 \cdot 10^{-1}$	$5.359 \cdot 10^{-1}$	$4.409 \cdot 10^{-1}$
max. $D$ (weak $\Delta\epsilon$ constraint)	$5.687 \cdot 10^{-1}$	$8.752 \cdot 10^{-1}$	$9.565 \cdot 10^{-1}$
max. $D$ (strong $\Delta\epsilon$ constraint)	$4.722 \cdot 10^{-1}$	$8.612 \cdot 10^{-1}$	$7.068 \cdot 10^{-1}$

### 3.1 Effect of initial replica positions on optimization results

It is natural to assume that increasing diversity of molecules initially occupied by replicas should make it easier for MOSAiCS to propose better candidate molecules. We tested this hypothesis on minimizing  $\Delta G_{\text{solv}}$  with strong  $\Delta\epsilon$  constraint over QM9\*, since it is a problem for which converged results proved easy to obtain and for which improvement over QM9 was observed. For that optimization problem we launched 8 simulations with  $\alpha_b = 0.0$  which only differed from the others presented in this work by the choice of initial molecules: each was chosen with uniform probability from molecules in the intersection of QM9 and QM9\* that

satisfied strong constraint on  $\Delta\epsilon^{\text{cheap}}$ , then initial molecules were assigned to replicas in such a way that molecules with larger  $\Delta G_{\text{solv}}^{\text{cheap}}$  were occupied by replicas with smaller  $\beta^{(i)}$ . The resulting mean optimization progress is plotted in Figure S14, with the corresponding values observed when all replicas were initialized in methane added for comparison. Surprisingly, while simulations with random starting molecules had significantly larger starting values of relative improvement, they failed to go beyond those values significantly earlier than simulations initialized with methane, and they all proposed previously mentioned  $\text{C}_2^{\text{QM9}}$  as the candidate. While there might be better ways to choose initial molecules that would make search for candidates tangibly faster, finding them was beyond the scope of this work.

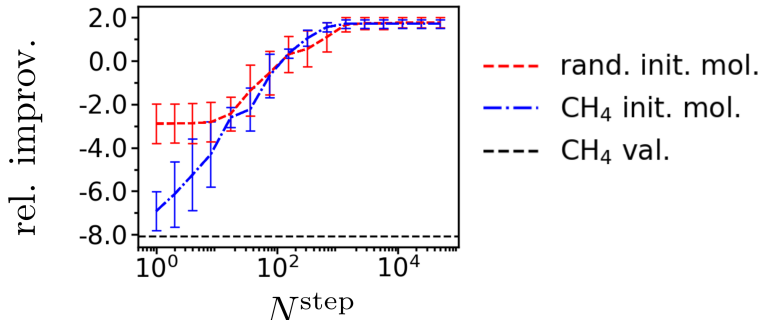


Figure S14: Relative improvement observed at  $N^{\text{step}}$  global Monte Carlo steps for QM9\* simulations optimizing  $\Delta G_{\text{solv}}$  with strong  $\Delta\epsilon$  constraint if the molecules initially occupied by replicas are chosen randomly from QM9 dataset (“rand. init. mol.”) with bias proportionality coefficient  $\alpha_b$  set to 0.0. Plotted for comparison are corresponding values when all replicas are initialized at methane (“CH<sub>4</sub> init. mol.”, also appearing in Figure S6a) as well as the relative improvement value for methane (“CH<sub>4</sub> val.”).

### 3.2 EGP\* full candidate list

EGP\* candidates proposed by MOSAiCS are listed in Tables S7-S10. Examples of candidates plotted in Figure S15 demonstrate MOSAiCS’ ability to produce candidates with complicated structures, including unusual heterocycles ( $\text{C}_{14}^{\text{EGP}}$ ,  $\text{C}_{38}^{\text{EGP}}$ , and  $\text{C}_{82}^{\text{EGP}}$ ), conjugated heterocycles ( $\text{C}_{17}^{\text{EGP}}$ ,  $\text{C}_{40}^{\text{EGP}}$ ), and caged molecules ( $\text{C}_{32}^{\text{EGP}}$ ).

Table S7: EGP\* candidates proposed during minimization of free energy of solvation  $\Delta G_{\text{solv}}$  with weak constraint on the HOMO-LUMO gap  $\Delta\epsilon$ , the corresponding values of  $\Delta G_{\text{solv}}$ , and the number of times a molecule was proposed as a candidate by simulations run with different values of the bias proportionality coefficient  $\alpha_b$  (prop. with  $\alpha_b$ ).

molecule	SMILES	$\Delta G_{\text{solv}}$ , kJ/mol	prop. with $\alpha_b$		
			0.0	0.2	0.4
$C_1^{\text{EGP}}$	<chem>CS(C)=P(C)(C)[Si](C)(Cl)S[Si]1=P[Si]1(Br)Br</chem>	$(-1.194 \pm 0.007) \cdot 10^3$	0	0	1
$C_2^{\text{EGP}}$	<chem>CS(C)(C)CCP1CS1=P(=O)SP(=O)=O</chem>	$(-1.080 \pm 0.001) \cdot 10^3$	0	1	2
$C_3^{\text{EGP}}$	<chem>CS(C)(C)CNP1CS1=P(=O)SP(=O)=O</chem>	$(-1.041 \pm 0.001) \cdot 10^3$	0	1	0
$C_4^{\text{EGP}}$	<chem>CS(C)(C)CC(Br)S[Si](Br)(Br)SP(=O)=O</chem>	$(-9.896 \pm 0.092) \cdot 10^2$	0	2	1
$C_5^{\text{EGP}}$	<chem>CS(C)(C)CNP1NS1=P(=O)SP(=O)=O</chem>	$(-9.868 \pm 0.050) \cdot 10^2$	0	0	1
$C_6^{\text{EGP}}$	<chem>CS(C)(C)CS[Si]1(Br)S[Si]1(Br)SP(=O)=O</chem>	$(-9.660 \pm 0.075) \cdot 10^2$	0	0	1
$C_7^{\text{EGP}}$	<chem>CS(C)(C)CP(Br)S[Si](Br)(Br)SP(=O)=O</chem>	$(-9.573 \pm 0.127) \cdot 10^2$	0	1	0
$C_8^{\text{EGP}}$	<chem>CS1(C)CCS(=P(=O)SP(=O)=O)P(Cl)C1</chem>	$(-9.556 \pm 0.055) \cdot 10^2$	0	1	0
$C_9^{\text{EGP}}$	<chem>CS(C)(C)CC(Cl)S[Si](Br)(Br)SP(=O)=O</chem>	$(-9.405 \pm 0.226) \cdot 10^2$	0	0	1
$C_{10}^{\text{EGP}}$	<chem>CS1(C)CCP(Cl)[Si](Br)(SP(=O)=O)SC1</chem>	$(-9.244 \pm 0.092) \cdot 10^2$	0	1	0
$C_{11}^{\text{EGP}}$	<chem>CS(=NP(=O)=S=P(=O)Br)NCS(C)(C)C</chem>	$(-8.418 \pm 0.102) \cdot 10^2$	0	1	0
$C_{12}^{\text{EGP}}$	<chem>CS(P1CSP(SP(=O)=O)S1)=P(C)(C)N</chem>	$(-7.724 \pm 0.026) \cdot 10^2$	0	0	1
$C_{13}^{\text{EGP}}$	<chem>CS(C)(C)CCSNP(=O)=CP(#N)Br</chem>	$(-7.144 \pm 0.056) \cdot 10^2$	1	0	0
$C_{14}^{\text{EGP}}$	<chem>CP1(=CN)CP(C)(N)=[Si](SP(=O)=O)S1</chem>	$(-5.121 \pm 0.076) \cdot 10^2$	1	0	0
$C_{15}^{\text{EGP}}$	<chem>CP1(N)=CP(SP(=O)=O)C(N)=P(C)(C)C1</chem>	$(-4.511 \pm 0.059) \cdot 10^2$	1	0	0
$C_{16}^{\text{EGP}}$	<chem>CP(C)(N)=C(N)NCOC(=N)SP(=O)=O</chem>	$(-4.456 \pm 0.079) \cdot 10^2$	1	0	0
$C_{17}^{\text{EGP}}$	<chem>CS(C)(C)N=CP1(N)=NP2(=NP(=O)=N2)O1</chem>	$(-4.261 \pm 0.003) \cdot 10^2$	1	0	0
$C_{18}^{\text{EGP}}$	<chem>CP(N)(N)=C1NCCOP(OP(=O)=O)N1</chem>	$(-4.153 \pm 0.006) \cdot 10^2$	1	0	0
$C_{19}^{\text{EGP}}$	<chem>CS(C)(=NCCS(#N)=NP(#N)Br)=C(N)N</chem>	$(-3.825 \pm 0.013) \cdot 10^2$	1	0	0
$C_{20}^{\text{EGP}}$	<chem>CP1(N)=C(N)P(OP(=O)=O)S(=O)CCC1</chem>	$(-3.822 \pm 0.012) \cdot 10^2$	1	0	0



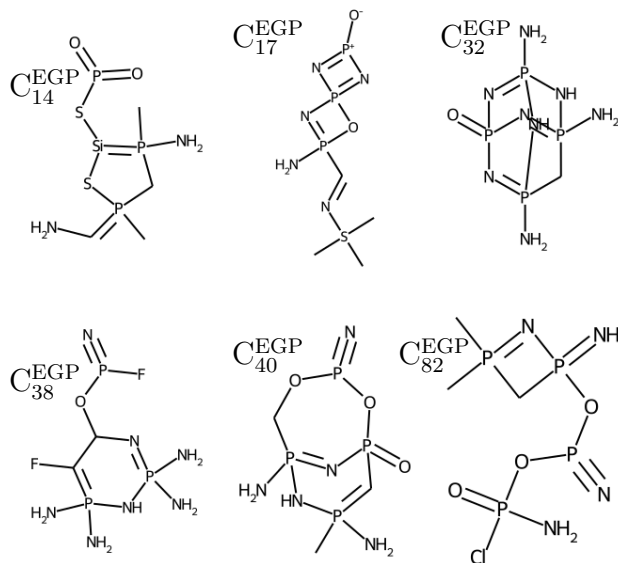


Figure S15: Examples of EGP\* candidates.

Table S8: EGP\* candidates proposed during minimization of free energy of solvation  $\Delta G_{\text{solv}}$  with strong constraint on HOMO-LUMO gap  $\Delta\epsilon$ ; columns are labeled analogously to Table S7.

molecule	SMILES	$\Delta G_{\text{solv}}$ , kJ/mol	prop. with $\alpha_b$		
			0.0	0.2	0.4
C <sub>21</sub> <sup>EGP</sup>	<chem>COP(#N)OP(#N)NCCP(N)(N)=CN</chem>	$(-2.698 \pm 0.021) \cdot 10^2$	1	0	0
C <sub>22</sub> <sup>EGP</sup>	<chem>N#P(N)OP(#N)OCNCP(N)(N)=CN</chem>	$(-2.670 \pm 0.043) \cdot 10^2$	1	1	0
C <sub>23</sub> <sup>EGP</sup>	<chem>CC(OCOP(#N)OP(#N)N)=P(C)(C)N</chem>	$(-2.483 \pm 0.037) \cdot 10^2$	0	1	0
C <sub>24</sub> <sup>EGP</sup>	<chem>CP(N)(=CN)NCNP(#N)OP(#N)N</chem>	$(-2.480 \pm 0.014) \cdot 10^2$	0	1	0
C <sub>25</sub> <sup>EGP</sup>	<chem>N#P(F)OP(#N)NP1(=N)NC=P(N)(N)N1</chem>	$(-2.431 \pm 0.013) \cdot 10^2$	0	1	0
C <sub>26</sub> <sup>EGP</sup>	<chem>CC(CP(N)(N)=CN)NP(#N)OP(#N)N</chem>	$(-2.405 \pm 0.051) \cdot 10^2$	1	0	0
C <sub>27</sub> <sup>EGP</sup>	<chem>CP(C)(N)=COCCOP(#N)OP(#N)N</chem>	$(-2.383 \pm 0.042) \cdot 10^2$	1	0	0
C <sub>28</sub> <sup>EGP</sup>	<chem>N#P(F)OP(#N)OC1CC(=P(N)(N)N)O1</chem>	$(-2.376 \pm 0.007) \cdot 10^2$	0	1	0
C <sub>29</sub> <sup>EGP</sup>	<chem>COP(#N)NP(#N)NCCP(N)(N)=CN</chem>	$(-2.368 \pm 0.023) \cdot 10^2$	1	0	0
C <sub>30</sub> <sup>EGP</sup>	<chem>CP(C)(C)=COC(N)OP(#N)OP(#N)N</chem>	$(-2.366 \pm 0.007) \cdot 10^2$	0	0	1
C <sub>31</sub> <sup>EGP</sup>	<chem>CP(C)(N)=C(F)OCOP(#N)OP(#N)F</chem>	$(-2.335 \pm 0.020) \cdot 10^2$	0	1	0
C <sub>32</sub> <sup>EGP</sup>	<chem>NP12=NP3(=O)N=P(N)(C1)NP(N)(=N3)N2</chem>	$(-2.295 \pm 0.008) \cdot 10^2$	0	1	0
C <sub>33</sub> <sup>EGP</sup>	<chem>N#P(F)OP1(=O)C=P(N)(N)CP(N)(N)=N1</chem>	$(-2.291 \pm 0.010) \cdot 10^2$	0	1	0
C <sub>34</sub> <sup>EGP</sup>	<chem>CP1(N)=CP(=O)(OP(#N)N)N=P(N)(N)N1</chem>	$(-2.261 \pm 0.027) \cdot 10^2$	0	0	2
C <sub>35</sub> <sup>EGP</sup>	<chem>CP12=NP3(=O)N=P(N)(CP(N)(=N3)N1)N2</chem>	$(-2.257 \pm 0.007) \cdot 10^2$	0	0	1
C <sub>36</sub> <sup>EGP</sup>	<chem>NP12=NP3(=O)N=P(N)(N1)NP(N)(=N3)N2</chem>	$(-2.253 \pm 0.008) \cdot 10^2$	0	0	1
C <sub>37</sub> <sup>EGP</sup>	<chem>CP(N)(N)=C1COP(#N)OP(N)(=O)N1</chem>	$(-2.232 \pm 0.007) \cdot 10^2$	2	0	1
C <sub>38</sub> <sup>EGP</sup>	<chem>N#P(F)OC1N=P(N)(N)NP(N)(N)=C1F</chem>	$(-2.142 \pm 0.005) \cdot 10^2$	0	0	1
C <sub>39</sub> <sup>EGP</sup>	<chem>N#P(N)OP1(=O)C=P(N)(N)OP(N)(N)=N1</chem>	$(-2.099 \pm 0.019) \cdot 10^2$	0	0	1
C <sub>40</sub> <sup>EGP</sup>	<chem>CP1(N)=CP2(=O)N=P(N)(COP(#N)O2)N1</chem>	$(-2.076 \pm 0.009) \cdot 10^2$	1	0	0

Table S9: EGP\* candidates proposed during maximization of dipole  $D$  with weak constraint on HOMO-LUMO gap  $\Delta\epsilon$ ; columns are labeled analogously to Table S7.

molecule	SMILES	$D$ , debye	prop. with $\alpha_b$		
			0.0	0.2	0.4
$C_{41}^{\text{EGP}}$	<chem>CS(C)(C)CCC=PSP(#N)SP(=O)=O</chem>	$(1.095 \pm 0.009) \cdot 10^2$	0	1	0
$C_{42}^{\text{EGP}}$	<chem>CS(C)(C)CSC=CSP(#N)SP(=O)=O</chem>	$(1.075 \pm 0.009) \cdot 10^2$	0	1	0
$C_{43}^{\text{EGP}}$	<chem>O=P(=O)SP(=O)=S1N[Si]1=S1CP1CSCl</chem>	$(1.063 \pm 0.013) \cdot 10^2$	0	1	0
$C_{44}^{\text{EGP}}$	<chem>CP(SC=CSCS(C)(C)C)SP(=O)=S</chem>	$(1.029 \pm 0.010) \cdot 10^2$	0	0	1
$C_{45}^{\text{EGP}}$	<chem>CP(NCNC(C)(C)C)SP(=O)=O</chem>	$(1.012 \pm 0.010) \cdot 10^2$	0	1	0
$C_{46}^{\text{EGP}}$	<chem>CP(SC=CSCS(C)(C)C)SP(=O)=O</chem>	$(9.944 \pm 0.077) \cdot 10^1$	0	1	0
$C_{47}^{\text{EGP}}$	<chem>CS(C)(C)CCCCNP(F)SP(=O)=O</chem>	$(9.743 \pm 0.127) \cdot 10^1$	0	1	0
$C_{48}^{\text{EGP}}$	<chem>CS(C)(C)CCCS1=[Si](SP(=S)=S)C1N</chem>	$(9.713 \pm 0.073) \cdot 10^1$	0	0	1
$C_{49}^{\text{EGP}}$	<chem>CS(C)(C)CCNSNP(#N)SP(=O)=O</chem>	$(9.640 \pm 0.238) \cdot 10^1$	0	0	1
$C_{50}^{\text{EGP}}$	<chem>CS(C)(C)CCCCSP(F)SP(=O)=O</chem>	$(9.563 \pm 0.060) \cdot 10^1$	0	1	0
$C_{51}^{\text{EGP}}$	<chem>CS(C)(C)N=PSCSCSN=P(=O)Br</chem>	$(9.499 \pm 0.044) \cdot 10^1$	0	1	0
$C_{52}^{\text{EGP}}$	<chem>C=S(C)CSCP1CS1=P(=O)SP(=O)=O</chem>	$(9.420 \pm 0.082) \cdot 10^1$	0	0	1
$C_{53}^{\text{EGP}}$	<chem>CS(C)(C)NC=CSP(N=S)SP(=O)=O</chem>	$(9.267 \pm 0.026) \cdot 10^1$	0	0	1
$C_{54}^{\text{EGP}}$	<chem>CP(CCCSP(=O)=O)CCS(C)(C)C</chem>	$(9.264 \pm 0.110) \cdot 10^1$	0	0	1
$C_{55}^{\text{EGP}}$	<chem>CS(C)(N)C[Si]1(F)CSP(SP(=O)=S)S1</chem>	$(8.639 \pm 0.076) \cdot 10^1$	0	0	1
$C_{56}^{\text{EGP}}$	<chem>C=S(C)(C)=PSC1OP1SCSP(=O)=O</chem>	$(8.447 \pm 0.059) \cdot 10^1$	0	0	1
$C_{57}^{\text{EGP}}$	<chem>CS(=CN)CCNCSP(#N)SP(#N)Br</chem>	$(7.938 \pm 0.134) \cdot 10^1$	1	0	0
$C_{58}^{\text{EGP}}$	<chem>CS1(CSC=CSP(#N)SP(#N)Br)CO1</chem>	$(7.709 \pm 0.071) \cdot 10^1$	1	0	0
$C_{59}^{\text{EGP}}$	<chem>C=S(C)(C)=PC=CCSC(=O)SP(=O)=O</chem>	$(7.685 \pm 0.093) \cdot 10^1$	1	0	0
$C_{60}^{\text{EGP}}$	<chem>CS(C)(=CC=COS(=O)P(=O)=S)=C(N)N</chem>	$(7.587 \pm 0.020) \cdot 10^1$	1	0	0
$C_{61}^{\text{EGP}}$	<chem>C=S(C)(=CN)CCCSP(#N)SP(#N)Br</chem>	$(7.495 \pm 0.137) \cdot 10^1$	1	0	0
$C_{62}^{\text{EGP}}$	<chem>CP(C)(C)=C(N)NC=CCNCP(=S)=S</chem>	$(7.457 \pm 0.087) \cdot 10^1$	1	0	0
$C_{63}^{\text{EGP}}$	<chem>CP(C)(NC=CNC#CP(=S)=S)=C(N)N</chem>	$(7.453 \pm 0.009) \cdot 10^1$	1	0	0
$C_{64}^{\text{EGP}}$	<chem>CS(C)(=CN)=NSCC=CN=S=NC=O</chem>	$(5.369 \pm 0.012) \cdot 10^1$	1	0	0

Table S10: EGP\* candidates proposed during maximization of dipole  $D$  with strong constraint on HOMO-LUMO gap  $\Delta\epsilon$ ; columns are labeled analogously to Table S7.

molecule	SMILES	$D$ , debye	prop. with $\alpha_b$		
			0.0	0.2	0.4
$C_{65}^{\text{EGP}}$	<chem>NC=P(N)(N)CCCCNCS(=O)=O</chem>	$(5.981 \pm 0.114) \cdot 10^1$	0	1	0
$C_{66}^{\text{EGP}}$	<chem>CP(C)(C)=CCCCOP(#N)OP(#N)F</chem>	$(4.870 \pm 0.027) \cdot 10^1$	0	5	0
$C_{67}^{\text{EGP}}$	<chem>N#P(N)OP(#N)NCNCP(N)(N)=CN</chem>	$(4.865 \pm 0.073) \cdot 10^1$	0	1	0
$C_{68}^{\text{EGP}}$	<chem>C=P(C)(C)CCNCP(#N)OP(#N)F</chem>	$(4.587 \pm 0.049) \cdot 10^1$	1	0	0
$C_{69}^{\text{EGP}}$	<chem>CP(C)(N)=C1CC(OP(#N)OP(#N)F)C1</chem>	$(4.401 \pm 0.084) \cdot 10^1$	0	1	0
$C_{70}^{\text{EGP}}$	<chem>C=P(C)(C)CCCOP(#N)OP(#N)F</chem>	$(4.024 \pm 0.038) \cdot 10^1$	1	0	0
$C_{71}^{\text{EGP}}$	<chem>C=P1(N)CC(OCOP(#N)OP(#N)F)C1</chem>	$(3.924 \pm 0.057) \cdot 10^1$	0	0	1
$C_{72}^{\text{EGP}}$	<chem>CC=P(C)(N)NCOP(#N)OP(#N)F</chem>	$(3.847 \pm 0.052) \cdot 10^1$	0	0	1
$C_{73}^{\text{EGP}}$	<chem>C=P(N)(N)C(N)CCNP(#N)OP(#N)F</chem>	$(3.842 \pm 0.099) \cdot 10^1$	0	0	1
$C_{74}^{\text{EGP}}$	<chem>C=P(C)(N)CNCOP(#N)OP(#N)F</chem>	$(3.777 \pm 0.035) \cdot 10^1$	0	0	2
$C_{75}^{\text{EGP}}$	<chem>C=P(C)(C)OCC(F)OP(#N)OP(#N)F</chem>	$(3.768 \pm 0.034) \cdot 10^1$	0	0	1
$C_{76}^{\text{EGP}}$	<chem>CP(N)(N)=CCCCCOCNP(#N)F</chem>	$(3.674 \pm 0.091) \cdot 10^1$	0	0	1
$C_{77}^{\text{EGP}}$	<chem>CC(CNP(=O)(F)NP(#N)F)=P(C)(C)N</chem>	$(3.427 \pm 0.070) \cdot 10^1$	0	0	1
$C_{78}^{\text{EGP}}$	<chem>CP(C)(N)=CCC(F)(F)CCOP(#N)F</chem>	$(3.195 \pm 0.048) \cdot 10^1$	1	0	0
$C_{79}^{\text{EGP}}$	<chem>C=P(C)(N)CCOP(#N)OCOP(#N)F</chem>	$(3.134 \pm 0.126) \cdot 10^1$	1	0	0
$C_{80}^{\text{EGP}}$	<chem>CC=P(C)(N)CC(F)CCOP(#N)F</chem>	$(2.977 \pm 0.052) \cdot 10^1$	1	0	0
$C_{81}^{\text{EGP}}$	<chem>N#P(F)NCCC12C=P(N)(NCN1)NC2</chem>	$(2.870 \pm 0.041) \cdot 10^1$	1	0	0
$C_{82}^{\text{EGP}}$	<chem>CP1(C)=NP(=N)(OP(#N)OP(N)(=O)Cl)C1</chem>	$(2.643 \pm 0.006) \cdot 10^1$	1	0	0
$C_{83}^{\text{EGP}}$	<chem>CP(C)(C)=N[Si]1(N)COC(OP(#N)F)C1</chem>	$(2.588 \pm 0.017) \cdot 10^1$	1	0	0

## References

- (S1) Ebejer, J.-P.; Morris, G. M.; Deane, C. M. Freely Available Conformer Generation Methods: How Good Are They? *J. Chem. Inf. Model.* **52**, 1146–1158.
- (S2) <https://kjelljorner.github.io/morfeus>.
- (S3) (a) Halgren, T. A. Merck molecular force field. I. Basis, form, scope, parameterization, and performance of MMFF94. *J. Comput. Chem.* **1996**, *17*, 490–519; (b) Halgren, T. A. Merck molecular force field. II. MMFF94 van der Waals and electrostatic parameters for intermolecular interactions. *J. Comput. Chem.* **1996**, *17*, 520–552; (c) Halgren, T. A. Merck molecular force field. III. Molecular geometries and vibrational frequencies for MMFF94. *J. Comput. Chem.* **1996**, *17*, 553–586; (d) Halgren, T. A.; Nachbar, R. B. Merck molecular force field. IV. Conformational energies and geometries for MMFF94. *J. Comput. Chem.* **1996**, *17*, 587–615; (e) Halgren, T. A. Merck molecular force field. V. Extension of MMFF94 using experimental data, additional computational data, and empirical rules. *J. Comput. Chem.* **1996**, *17*, 616–641; (f) Halgren, T. A. MMFF VI. MMFF94s option for energy minimization studies. *J. Comput. Chem.* **1999**, *20*, 720–729; (g) Halgren, T. A. MMFF VII. Characterization of MMFF94, MMFF94s, and other widely available force fields for conformational energies and for intermolecular-interaction energies and geometries. *J. Comput. Chem.* **1999**, *20*, 730–748.
- (S4) Tosco, P.; Stiefl, N.; Landrum, G. Bringing the MMFF force field to the RDKit: implementation and validation. *J. Cheminform.* **2014**, *6*, 37.
- (S5) RDKit: Open-source cheminformatics. <https://www.rdkit.org>.
- (S6) Kim, Y.; Kim, W. Y. Universal Structure Conversion Method for Organic Molecules: From Atomic Connectivity to Three-Dimensional Geometry. *BKCS* **2015**, *36*, 1769–1777.

- (S7) <https://github.com/jensengroup/xyz2mol>.
- (S8) Bannwarth, C.; Caldeweyher, E.; Ehlert, S.; Hansen, A.; Pracht, P.; Seibert, J.; Spicher, S.; Grimme, S. Extended tight-binding quantum chemistry methods. *WIREs Computational Molecular Science* **2021**, *11*, e1493.
- (S9) Bannwarth, C.; Ehlert, S.; Grimme, S. GFN2-xTB-An Accurate and Broadly Parametrized Self-Consistent Tight-Binding Quantum Chemical Method with Multipole Electrostatics and Density-Dependent Dispersion Contributions. *J. Chem. Theory Comput.* **2019**, *15*, 1652–1671.
- (S10) Ehlert, S.; Stahn, M.; Spicher, S.; Grimme, S. Robust and Efficient Implicit Solvation Model for Fast Semiempirical Methods. *J. Chem. Theory Comput.* **2021**, *17*, 4250–4261.
- (S11) Chung, Y.; Gillis, R. J.; Green, W. H. Temperature-dependent vapor–liquid equilibria and solvation free energy estimation from minimal data. *AIChE J.* **2020**, *66*, e16976.